ELSEVIER

Journal of Molecular Catalysis A: Chemical 173 (2001) 135–184

JOURNAL OF MOLECULAR CATALYSIS A: CHEMICAL

www.elsevier.com/locate/molcata

Membrane reactors for hydrogenation and dehydrogenation processes based on supported palladium

Roland Dittmeyer [a,*], Volker Höllein [a], Kristian Daub [b]

[a] *DECHEMA e.V., Karl-Winnacker-Institut, Theodor-Heuss-Allee 25, 60486 Frankfurt am Main, Germany*
[b] *Universität Erlangen-Nürnberg, Lehrstuhl für Technische Chemie I, Egerlandstraße 3, 91058 Erlangen, Germany*

Abstract

Membrane reactors applied to catalytic reactions are currently being studied in many places world-wide. Significant developments in membrane science and the vision of process intensification by multifunctional reactors have stimulated a lot of academic and industrial research, which is impressively demonstrated by more than 100 scientific papers on catalytic membrane reactors being published per year. Palladium as a noble metal with exceptional hydrogen permeation properties and, at the same time, broad applicability as a catalyst, first of all for hydrogenation, is part of many of these developments.

This paper discusses two different membrane reactor concepts which both rely on supported palladium, on the one hand as a permselective membrane material, and on the other hand as base component of a membrane-type hydrogenation catalyst. Dense palladium composite membranes can be used for hydrogen separation from packed-bed catalysts in gas-phase hydrocarbon dehydrogenation reactions. Mesoporous membranes containing dispersed bimetallic Pd/X-clusters can be employed as so-called *catalytic diffusers* for liquid-phase hydrogenation, e.g. of nitrate and nitrite in water. The principles of both concepts are introduced, recently obtained experimental data are evaluated in connection with literature results, and the perspectives for further development are highlighted.

Keywords: Membrane reactor; Composite palladium membrane; Catalytic membrane; Palladium catalyst; Liquid-phase hydrogenation; Gas-phase hydrocarbon dehydrogenation

1. Membrane reactor concepts

According to the IUPAC definition a membrane reactor is a device that combines a membrane-based separation process with a chemical reaction step in one unit. Various possibilities exist for such a combination. The most widely used concept is the selective removal of products from the reaction zone (cf. Fig. 1a), which is applied first of all to equilibrium limited reactions to increase the yield beyond the corresponding equilibrium value, or, generally speaking, to repress undesired secondary reactions of the prod-

Abbreviations: CMR, catalytic membrane reactor; CNMR, catalytic non-permselective membrane reactor; CSTR, continuous stirred tank reactor; CVD, chemical vapour deposition; FBCMR, fluidised-bed catalytic membrane reactor; FBMR, fluidised-bed membrane reactor; GHSV, gas hourly space velocity (m^3 feed/m^3 catalyst h); HVOF, high-velocity oxy-fuel flame spraying; IMCR, inert membrane catalytic reactor; IMR, inert membrane reactor; LHSV, liquid hourly space velocity (m^3 feed/m^3 catalyst h); MOCVD, metal organic chemical vapour deposition; PBCMR, packed-bed catalytic membrane reactor; PBMR, packed-bed membrane reactor; PEM, proton exchange membrane; PVAL, polyvinyl alcohol; PVD, physical vapour deposition; S/O, steam to oil ratio (kg/kg or mol/mol); SS, stainless steel, weighted sum of squares defined by Eq. (12); WHSV, weight hourly space velocity (kg feed/kg catalyst h)

*Corresponding author. Tel.: +49-69-7564428; fax: +49-69-7564388.
E-mail address: dittmeyer@dechema.de (R. Dittmeyer).

1381-1169/01/$ – see front matter
PII: S1381-1169(01)00149-2

Nomenclature

a_V	membrane area per unit volume (m^{-1})
c_i	concentration of species i (mol/m^3)
E_A	activation energy (kJ/mol)
$H_{c,i}$	Henry constant (mol/m^3 Pa)
ΔH_R	enthalpy of reaction (kJ/mol)
J	hydrogen flux (mol/m^2 s)
k	reaction rate constant (mol/m^3 s Pa)
k_a	adsorption rate constant (mol/m^2 s Pa)
k_d	desorption rate constant (mol/m^2 s)
K_i	adsorption equilibrium constant of species i (Pa^{-1})
K_p	reaction equilibrium constant (Pa)
l	membrane thickness (m)
m_{Pd}	mass of palladium (mg)
M_i	molecular weight of species i (kg/kmol)
n	hydrogen pressure exponent
n_d, n_m	number of experiments and number of membranes, respectively (cf. Eq. (12))
$\dot{n}_i$	molar flow rate of species i (mol/s)
p_C	capillary pressure (Pa)
p_i	partial pressure of species i (Pa)
q	exponent of the adsorption term in Eq. (15)
Q	permeability (mol m/m^2 s Pa^n)
Q^*	permeability (related to the surface coverage by hydrogen) (mol m/m^2 s)
Q_0	prexponential factor of Q (mol m/m^2 s Pa^n)
r	reaction rate (mol/m^3 s)
$\bar{r}$	overall adsorption rate (mol/m^2 s)
r_P	pore radius (m)
R	universal gas constant (J/mol K)
R_i	rate of formation or consumption of species i (mol/m^3 s)
$S_{i,j}$	selectivity of species i based on element j
t	residence time (s)
T	temperature (K, °C)
V_R	packed-bed volume (m^3)
X_i	conversion of species i

Greek letters

α	contact angle (°)
δ	layer thickness (m)
ν_i	stoichiometric coefficient of species i
θ/θ_i	fractional coverage by vacant sites/species i
ρ_b	packed-bed density (kg/m^3)
σ	surface tension (mN/m)
τ	residence time (s)

Subscripts

0	initial, inlet
*	phase boundary, related to surface coverage, ideal membrane reactor
cat	catalyst
eq	equilibrium
exp	experimental
gas	gas
liq	liquid
m	mass
P	permeate
R	retentate
S	support

Superscript

e	end, exit

ucts. In a different approach only particular reactants are supplied selectively via a membrane to the reaction zone (cf. Fig. 1b), e.g. to establish an optimum concentration profile along the reactor. A third concept refers to a membrane that creates a well-defined reaction interface (or region) between two reactant streams (cf. Fig. 1c).

The mass transport across a membrane can be permselective if only some components of a mixed stream permeate through the membrane (cf. Fig. 1a and b) or non-permselective if all species permeate at comparable rates (cf. Fig. 1c). Permselective transport is found first of all in dense membranes. It is governed by a solution-diffusion mechanism. Non-permselective transport normally occurs in macro- and mesoporous membranes. In the latter Knudsen diffusion is often the dominating transport mechanism. Microporous membranes represent a bit of both: permselective and non-permselective transport is possible depending on the size of the permeating molecules in view of the pore size of the membrane (bottlenecks) as well as on the chemical nature of the permeating molecules and the membrane material.

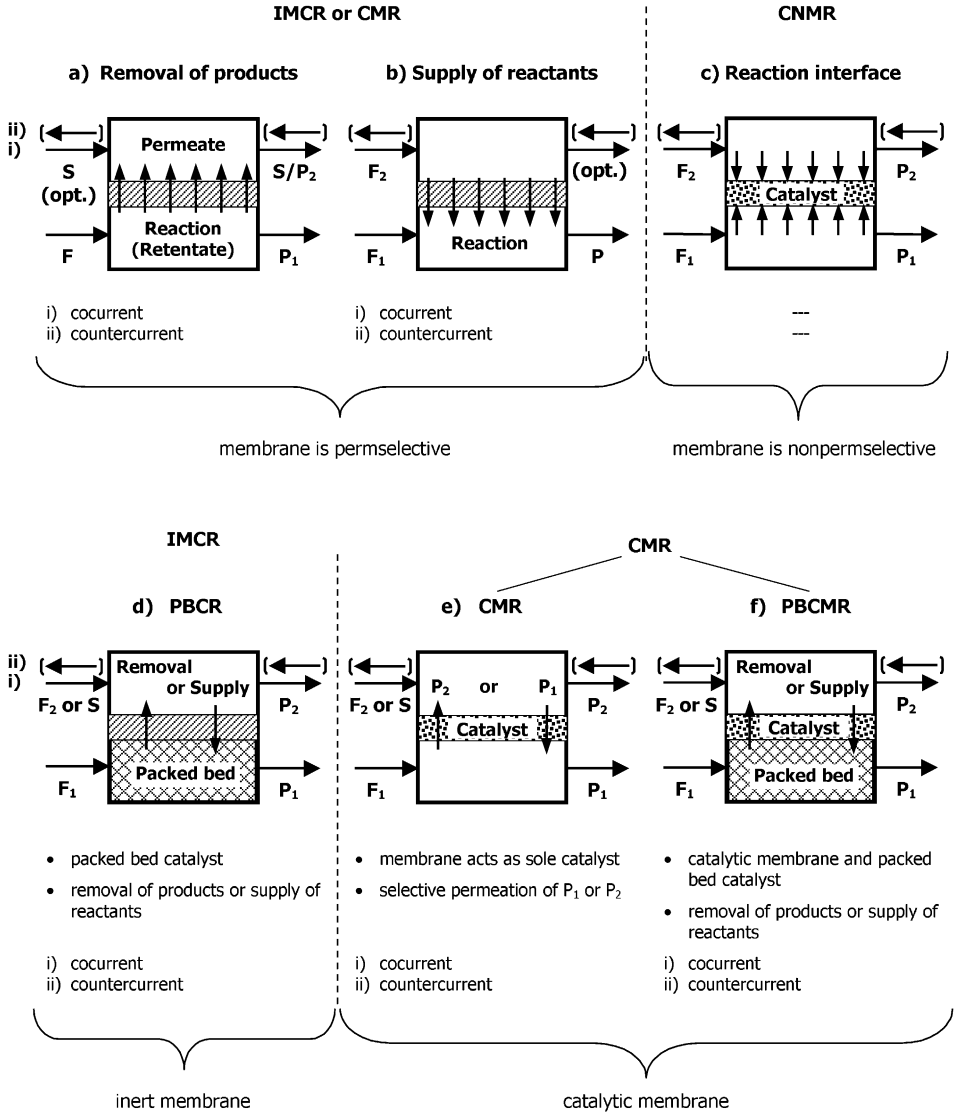

Fig. 1. Classification of membrane reactor concepts according to the membrane functions.

When the membrane reactor is used for carrying out a catalysed reaction the questions arises whether the membrane itself has a catalytic function or not. If the membrane acts as a catalyst we refer to this as a catalytic membrane reactor (CMR, cf. Fig. 1e and f), if not we have an inert membrane catalytic reactor (IMCR, cf. Fig. 1d). The CMR-case may be further subdivided into two categories, i.e. when the membrane acts as the sole catalyst (cf. Fig. 1e), and when a conventional catalyst is present in addition to the membrane (cf. Fig. 1f).

Other authors have introduced similar acronyms for an easy reference to the different membrane reactor types. Tsotsis et al. [1] refer to a catalytic

non-permselective membrane reactor (CNMR) as to a reactor with a catalytic membrane which is not permselective but provides for a well-defined interface for two (or more) reactants flowing on opposite sides of the membrane (cf. Fig. 1c). In contrast their definition of a catalytic membrane reactor (CMR) requires a permselective membrane (cf. Fig. 1e). In both cases the membrane acts as the sole catalyst. The same authors assigned the acronyms PBMR and FBMR to the packed-bed and fluidised-bed membrane reactor where the membrane is permselective but not catalytic (cf. Fig. 1d). The opposite cases, i.e. with catalytic and permselective membrane, are referred to as PBCMR and FBCMR, respectively (cf. Fig. 1f). Coronas and Santamaria [2] used the notations CMR and IMR to distinguish between the catalytic and the inert membrane reactor. According to their definition the CMR has no other type of catalyst except the membrane. Consequently a third category "combined" is introduced to refer to membrane reactor configurations where the catalyst is placed both inside and outside the membrane. No further distinction is made in view of the permselectivity, i.e. whether the membrane performs a separation task, whether it provides a reaction interface for different reactant streams, or whether it acts only as a special type of catalyst support, e.g. to minimise the mass transport resistance when the whole feed stream is passed through it in cross-flow.

In the past 15 years many valuable reviews on membrane reactors have been published [1–21]. It is not the intention of this paper to add one more to the list but rather to emphasise the use of palladium in this field.

2. Membrane reactors based on palladium alloy membranes

It is well established that dense palladium and palladium alloy membranes are permeable for hydrogen only. Two main possibilities arise from this feature to employ these in membrane reactors, namely

1. to promote a dehydrogenation reaction by removal of the produced hydrogen from a dehydrogenation catalyst through the membrane, i.e. preventing the establishment of the chemical equilibrium, or
2. to carry out a hydrogenation reaction on the palladium surface with supply of hydrogen through the membrane.

The purpose of the use of the palladium membrane as well as its function differs considerable in both types of applications. In case (1) the aim is to increase the conversion of an equilibrium limited reaction by removal of one of the products. The dehydrogenation occurs in the gas phase over a conventional catalyst (e.g. a packed-bed) which is surrounded by the palladium membrane. In principle the palladium surface could act as a dehydrogenation catalyst too, but then the reaction rate would be too small due to the low surface area. Hence, the membrane has no primary catalytic function. In case (2) the purpose can be two-fold: to promote a selective hydrogenation by deliberately dosing hydrogen through the membrane, or to utilise an existing diluted hydrogen gas to perform the hydrogenation. In both situations the palladium membrane has a catalytic function.

From an engineering point of view case (2) has a limited potential, at least for gas-phase hydrogenations. It is true that palladium is a versatile hydrogenation catalyst, but the reaction rate normally is proportional to the surface area of the catalyst, provided no diffusion limitation occurs and the active sites are uniformly distributed over the surface. Conventional hydrogenation catalysts have the palladium in highly dispersed form, e.g. as nanoscale metal clusters inside a porous pellet, and hence do offer a large palladium surface area. Compared to this the accessible surface area of a dense palladium membrane is small.

If the hydrogenation is to be performed in the liquid phase the situation may be different because then the reaction rate is often controlled by the kinetics of hydrogen mass transfer, and the available active surface inside the porous catalyst is utilised anyway only in part. Liquid-phase hydrogenations are carried out at high pressure due to the poor solubility of hydrogen in most organic liquids. Palladium membranes would allow for a simplification of the process design, as they could take over both the catalytic function and the task of dosing hydrogen. High pressure operation could then be avoided. Combined with a clear benefit in selectivity there might be interesting applications of this concept in the fine chemicals area. However, most of the recent studies using palladium-based membranes in literature are aimed at hydrogen removal from packed-bed catalysts either to boost the yield of industrially important dehydrogenation reactions (propane, isobutane/*n*-butane, ethylbenzene, etc.) or to

provide pure hydrogen (steam reforming of methane or methanol, water-gas-shift reaction), e.g. for use in low-temperature (PEM) fuel cell stacks. Hence, the discussion here is restricted to this type of application only.

2.1. Working principle of a inert membrane catalytic reactor with removal of hydrogen

The principle of a hydrogen permselective membrane reactor equipped with a packed-bed of catalyst and a surrounding palladium-based membrane has been described many times in literature. Fig. 2 illustrates the situation. The dehydrogenation occurs on the packed-bed catalyst, and the produced hydrogen is withdrawn through the membrane. The transport through the membrane is driven by the hydrogen partial pressure difference between the packed-bed (i.e. retentate) side and the permeate side. Three different possibilities exist to create the driving force:

1. Use of an inert sweep gas in the permeate compartment (e.g. nitrogen, helium, etc.).
2. Application of a pressure difference between retentate and permeate compartment (if necessary by evacuation of the permeate).
3. Use of a reactive sweep gas to consume the permeated hydrogen (e.g. oxygen, air, carbon monoxide, unsaturated hydrocarbons, etc.).

Which of these possibilities is the best depends on the particular situation. In general, the worst case is the inert sweep gas because this has to be provided and compressed, and a diluted hydrogen gas is produced which can be used only as a fuel gas with low calorific value. If the kinetics of the hydrogen producing reaction do allow an operation at elevated pressure, for instance in the range of 1–3 MPa, this becomes an attractive option because then the pressure difference is sufficiently large to flush out the permeated hydrogen. The advantages are that no sweep gas is required and that pure hydrogen is obtained as a marketable product. On the other hand, the feed gas has to be compressed but the produced hydrogen is obtained at low pressure, which limits its usability and could make a recompression necessary. If pure hydrogen, e.g. for a fuel cell, is the target product of the membrane reactor, then an operation at elevated retentate pressure is the only viable option. The third option, i.e. reacting the permeated hydrogen with the sweep gas, is promising because it avoids the disadvantages of the other two. Moreover, since hydrogen producing reactions are endothermic in most cases (hydrocarbon dehydrogenation and hydrocarbon steam reforming) it is favourable to generate the required heat right in the permeate compartment. An exothermic hydrogen-consuming reaction can be carried out for this purpose, if possible employing the palladium membrane surface as a catalyst. Hydrogen oxidation with air or hydrogenation of an organic compound are candidates if they fit with the required reactor temperature. The disadvantage of hydrogen oxidation is that a high-valued product is used to heat the dehydrogenation. The other case, coupling of the dehydrogenation process to a second synthesis, is difficult to run at optimised conditions in a commercial-scale reactor because of the reduced degree of freedom.

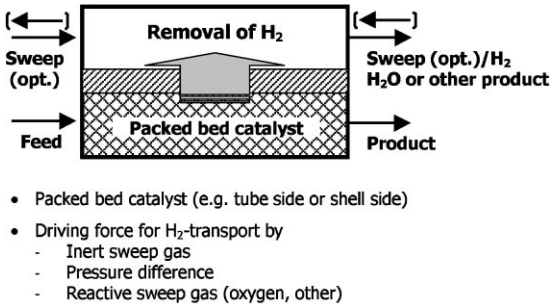

Fig. 2. Schematic of an inert membrane catalytic reactor equipped with a conventional packed-bed catalyst.

2.2. Development of palladium-based membranes

First investigations of the hydrogen absorption and diffusion through palladium were reported by Graham in 1866 [22]. Today it is well known that hydrogen permeates with an infinite selectivity via a solution-diffusion mechanism through palladium and its alloys. The permeation is based on a multi-step process. First molecular hydrogen is adsorbed on the palladium surface, where the dissociation into atomic hydrogen takes place. Then the hydrogen atoms enter the palladium lattice and diffuse through the lattice, while the electrons interact with the metal lattice. On the adjacent side the hydrogen atoms leave the lattice

and recombine on the surface, before they are finally desorbed as hydrogen molecules [23].

It is also well known that the use of pure palladium membranes is hindered by the fact that palladium shows a transition from the α-phase (hydrogen-poor) to the β-phase (hydrogen-rich) at temperatures below 300°C and pressures below 2 MPa, which depends on the hydrogen concentration in the metal. Since the lattice constant of the β-phase is 3% larger than that of the α-phase this transition leads to lattice strain and, consequently, after a few cycles to a distortion of the metal lattice [24]. Alloying the palladium, especially with silver, reduces the critical temperature for this embrittlement and leads to an increase of the hydrogen permeability. A maximum value of the hydrogen flow is reached for an alloy with approximately 23 wt.% silver [25,26]. Similar to Pd/Ag, other alloys, e.g. Pd/Y or Pd/Ce show high hydrogen permeability and good mechanical stability [27].

Palladium-based membranes have been used for decades to provide ultra-pure hydrogen, e.g. in the semiconductors industry and for the operation of fuel cells [28,29]. They were exploited to extract tritium from liquid-metal tritium breeders [30]. In recent years there has been a growing interest in the industrial application of palladium-based membranes for hydrogen producing reactions. Extensive investigations were conducted for the employment of palladium-based membranes for hydrogen removal to shift thermodynamic (equilibrium) limitations towards higher conversions, e.g. during dehydrogenation of hydrocarbons [31–33], steam reforming of methane [34–36] and the water-gas-shift reaction [37]. And it was shown that hydrogen feeding through palladium membranes can improve the selectivity of hydrogenation reactions [38]. Key requirements for the successful development of palladium-based membranes are low costs as well as high hydrogen permeability and permselectivity combined with good mechanical/thermal and long-term stability.

2.2.1. Dense palladium-based membranes

Early work focused on the application of relatively thick unsupported dense metal membranes prepared by conventional metallurgical processes. In 1964 Johnson Matthey developed a hydrogen purification equipment which employed a Pd/Ag tube [39]. However, the use of these membrane reactors is limited by the low hydrogen flow which is inversely proportional to the thickness of the membrane. Self supporting dense palladium-based membranes possess wall thicknesses greater than 50–100 μm to keep a sufficient mechanical strength. These membranes are too thick to obtain a satisfactory hydrogen flux. Besides the low permeance, thick palladium membranes are too expensive for an economic use, in particular since the price of palladium has tremendously increased over the last few years. For practical use it is necessary to reduce the thickness of the palladium layer. Composite metal membranes and composite porous membranes seem to be an advisable choice to overcome these disadvantages.

2.2.2. Palladium-based composite metal membranes

Palladium-based composite metal membranes consist of a thin layer of palladium or a palladium alloy coated on one or both sides of a hydrogen permeable base refractory metal such as niobium, vanadium or tantalum. These metals possess a high mechanical strength and are less expensive than palladium. Furthermore, the hydrogen flow through these body-centred cubic metals is higher than through the face-centred cubic palladium [40,41]. Unfortunately the direct replacement of palladium for these metals is not possible due to the formation of oxide layers and to surface reactions which reduce the hydrogen flow through the membrane [42]. In 1967 Makrides et al. [43] filed a patent for plating foils of Group VB metals with thin layers of palladium using sputter deposition. However, it has been reported that the hydrogen flux through palladium-based composite metal membranes decreases with time at high temperatures. Intermetallic diffusion between the metal layer and the base metal is the most likely reason for this notice [44]. To overcome this problem it was suggested to use a diffusion barrier between the base and the coating metal, e.g. thermal stable oxide layers such as alumina [44,45].

2.2.3. Palladium-based composite porous membranes

Palladium-based composite porous membranes consist of a thin dense layer of palladium or a palladium alloy on a porous support. Tubes or discs of porous glass, porous ceramics or porous stainless steel can all be employed as supports. Different techniques

such as chemical vapour deposition [46,47], magnetron sputtering [46,48], electrodeposition [49] and spray pyrolysis [50] have demonstrated the ability to coat palladium-based films on porous substrates [51]. Each method has its advantages. However, due to its simplicity, relatively low costs and uniformity of the deposition, electroless plating is the most popular and most successful procedure so far [52–55]. It is based on the autocatalytic reduction of a metastable metallic salt complex on an activated substrate surface. New preparation methods combine the electroless plating with reverse osmosis to obtain composite membranes with better thermal stability and higher permeance [56,57]. Excellent results have been reported recently for ultrathin composite membranes prepared by a modified electroless plating method, where the classical substrate surface activation has been replaced by a new photocatalytic deposition method [58,59].

2.3. Experimental

2.3.1. Preparation of palladium-based composite membranes

Many academic and industrial groups have developed palladium-based composite membranes in research projects, but so far no such products are available on a normal commercial basis. For our studies on the dehydrogenation of hydrocarbons in palladium membrane reactors we too have looked at different techniques for the manufacture of hydrogen permselective palladium and palladium–silver composite membranes. Details are reported in [60,61]. For the results presented in this paper mainly electroless plating was used. Asymmetric sintered porous stainless steel tubes supplied by GKN Sinter Metals Krebsöge Filters GmbH, Radevormwald (Germany), and asymmetric porous α-alumina tubes purchased from Inocermic GmbH, Hermsdorf (Germany), were employed as supports for the palladium plating. Both types have the same outer diameter of 10 mm and a comparable inner diameter of 6.5 mm for the sintered metal tubes and 7 mm for the ceramic tubes. The sintered metal tubes consist of two layers with different pore size. The nominal pore diameter of the fine layer, located on the shell side, is around 500 nm. The ceramic tubes have four layers with graded pore size. The finest layer has a mean pore diameter of 100 nm. The palladium was deposited always onto the layer with the finest pores.

The porous substrates were first cut to 11 cm length and cleaned with ammoniac solution, isopropyl alcohol and de-ionised water. Following the cleaning the substrate surface was seeded with Pd nuclei, which initiates the auto-catalytic reduction of the palladium complex in the subsequent plating step. For this purpose the tubes were successively immersed at ambient temperature in a tin chloride solution followed by an acidic palladium chloride bath. This sequence was repeated 10 times. Afterwards the palladium deposition was carried out at 60°C in a plating bath containing a palladium–amine complex as palladium source, hydrazine as reducer and EDTA as stabilising agent (cf. Table 1). The plating solution was changed every hour to keep the plating rate constant. Palladium deposition occurred according to Eq. (1).

$$2Pd^{2+} + N_2H_4 + 4OH^- \rightarrow 2Pd + N_2 + 4H_2O \quad (1)$$

After the plating the membranes were rinsed with de-ionised water and dried overnight at 120°C in a drying oven.

Palladium–silver composite membranes were prepared by successive deposition of palladium and silver on the porous supports followed by a heat treatment [53]. The first step was the preparation of a palladium layer as described above. Afterwards silver was deposited on the palladium film also by the electroless plating technique, which leads to the formation of a thin double layer of palladium and silver on the porous tube. The silver plating solution consisted mainly of an EDTA stabilised silver–amine complex with hydrazine as reducing agent (cf. Table 1). Silver

Table 1
Composition of the electroless plating baths for Pd and Ag and plating conditions

	Pd-bath	Ag-bath
Concentrations		
$PdCl_2$ (g/l)	5	0.5
$AgNO_3$ (g/l)	–	5
$Na_2EDTA{\cdot}2H_2O$ (g/l)	70	35
NH_4OH (28%) (ml/l)	500	500
$N_2H_4{\cdot}H_2O$ (ml/l)	10	5
pH value	10	10
Temperature (°C)	60	50

deposition occurred according to Eq. (2).

$$4Ag^{+} + N_2H_4 + 4OH^{-} \rightarrow 4Ag + N_2 + 4H_2O \quad (2)$$

After the plating the membranes were heated up to 700°C for 12 h under an atmosphere of argon. These high temperatures lead to the formation of a homogeneous palladium–silver film by thermal diffusion [53].

The thickness of the palladium and palladium–silver layers was determined from SEM micrographs and from the weight difference before and after the plating combined with the densities of the metals and under the assumption of uniform coverage.

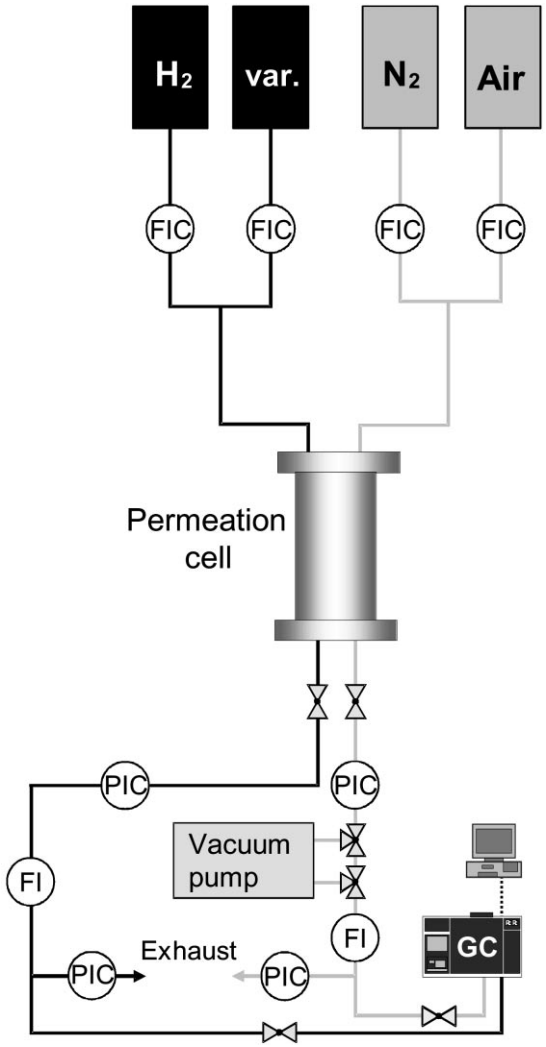

Fig. 3. Basic layout of the laboratory permeation apparatus.

2.3.2. Permeation measurements

The separation behaviour of the palladium composite membranes was investigated in the permeation apparatus shown schematically in Fig. 3. Details of the permeation unit are given in Fig. 4. The experiments were conducted with pure hydrogen and pure nitrogen as well as with a binary gas mixture of hydrogen with nitrogen. The temperature was varied between 350 and 650°C, and the pressure difference reached up to 400 kPa. Measurements were carried out with no sweep gas at atmospheric or low pressure on the permeate side and with nitrogen as sweep gas at atmospheric pressure. The heating rate was 1 K/min and below 300°C both sides of the membrane were kept under nitrogen to avoid hydrogen embrittlement. The desired feed gases were introduced with the aid of thermal mass flow controllers. The pressures on the retentate and permeate sides of the membrane were adjusted with back pressure controllers. The axial temperature profile of the reactor was monitored with thermocouples. The temperature variation over the whole length of the membrane did not exceed ±4°C. The gas flows leaving the reactor were measured by a thermal mass flow meter or a digital soap bubble flow meter. A gas

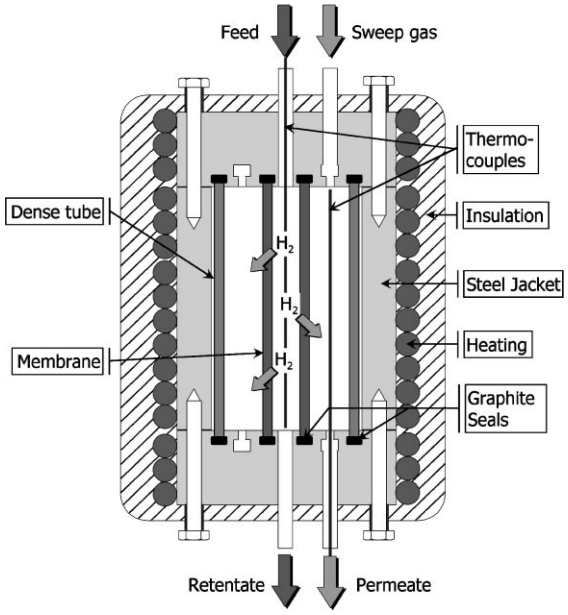

Fig. 4. Set-up of the permeation cell for measurements up to 650°C.

chromatograph was used to analyse the composition of the permeate and the retentate. The membrane was installed in the reactor by sealing both ends of the tube with graphite rings.

2.4. Results and discussion

2.4.1. Characterisation of the composite membranes by SEM

The surface morphology of an electroless deposited palladium film is shown in Fig. 5. It can be seen that the palladium film is composed of fine palladium grains. These grains are grown well together and form a dense palladium layer on the support. The minimum thickness of the palladium layer must be about 3 μm or greater with the above technique to get layers without pinholes. Fig. 6 shows a SEM micrograph of a palladium–silver surface after the final heat treatment. X-ray diffraction patterns of the surface of this membrane before (a) and after (b) the heat treatment are given in Fig. 7. After the plating the reflection peaks of pure silver and pure palladium can be seen among the peaks of the alumina support. After the heat treatment the peaks of the pure metals have disappeared and peaks of the palladium–silver alloy can be observed. These peaks lie between those for silver and palladium and shift with higher palladium contents to higher diffraction angles.

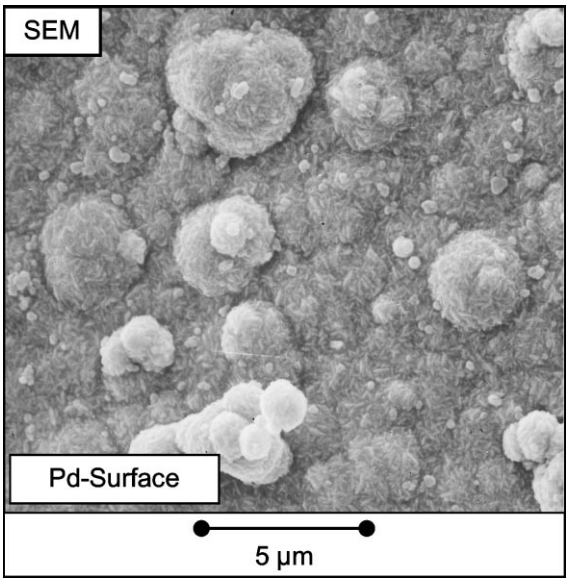

Fig. 5. Surface fine structure of a palladium layer deposited on an α-alumina support by electroless plating.

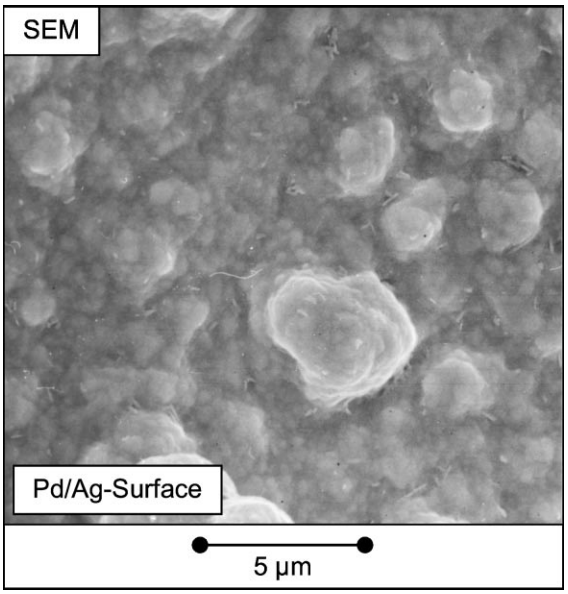

Fig. 6. Surface view of a palladium–silver layer deposited by electroless plating on an α-alumina support after the final heat treatment for 12 h at 700°C in an argon atmosphere.

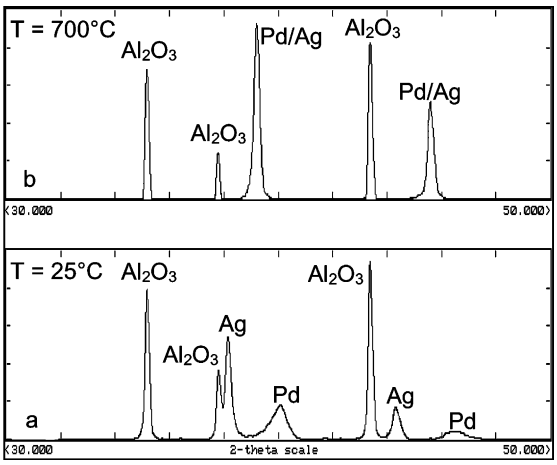

Fig. 7. XRD patterns of a palladium–silver layer after successive plating of palladium and silver (a), and after the final heat treatment for 12 h at 700°C in an argon atmosphere (b).

2.4.2. Permeation behaviour of the composite membranes

The quality of the prepared membranes was first examined by a simple pressure hold test at ambient temperature with nitrogen using gas-tight polymeric seals. At pressure differences up to 400 kPa the nitrogen flow through composite membranes with palladium layers thicker than 3 μm was negligible, i.e. less than 0.01 ml/cm^2 min (STP). This confirms that the palladium layers have very few defects.

As mentioned before the hydrogen diffusion through palladium occurs via a solution/diffusion mechanism. This transport is frequently described by Eq. (3) as follows:

$$J = \frac{Q}{l}(p_{HR}^n - p_{HP}^n) \quad (3)$$

where J is the *flux* of hydrogen, Q is the *permeability*, l denotes the thickness of the palladium layer, p_{HR} and p_{HP} stand for the hydrogen partial pressure in the permeate and retentate, and n is the *hydrogen pressure exponent*. The quotient Q/l is referred to as *permeance* or pressure normalised flux. The expression in parenthesis gives the *driving force* for the permeation. The value of n is often used as an indicator for the rate-controlling step of the permeation through a metal composite membrane. If the diffusion of atomic hydrogen through the dense metal layer is rate-limiting, then the hydrogen flow is directly proportional to the difference of the square root of the hydrogen partial pressure on both sides of the membrane (Sieverts's law) [25].

Figs. 8 and 9 illustrate the results of permeation experiments with pure gases. The hydrogen flow and the nitrogen flow through a palladium–alumina membrane is shown as a function of temperature for pressure differences between retentate and permeate up to 250 kPa. The palladium layer of the membrane was about 15 μm thick. No sweep gas was used, and the pressure on the permeate side was kept at atmospheric level (105 kPa). The hydrogen flow increases with rising temperature and transmembrane pressure difference. The nitrogen flow remains nearly unchanged with temperature but increases also with higher pressure difference. Under the same conditions the hydrogen flow is much higher than the nitrogen flow. Yet the nitrogen flow measured in the permeation cell is even at ambient temperature about 10–80 times higher

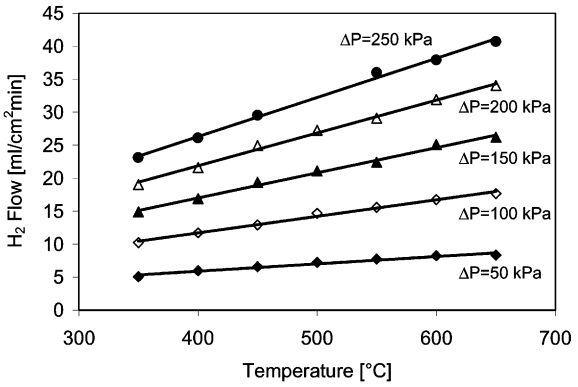

Fig. 8. Hydrogen flow through a 15 μm thick palladium–alumina membrane as a function of temperature for various pressure differences between retentate and permeate; single-gas hydrogen experiments without sweep gas; retentate pressure ranging from 155 to 355 kPa; fixed permeate pressure of 105 kPa.

than that detected in a pressure hold test with polymeric seals. This indicates that the graphite seals are not perfectly tight, i.e. the major part of the nitrogen flow shown in Fig. 9 does not pass through defects in the membrane layer but through small leaks at the seals.

The values detected for the hydrogen pressure exponent generally range between 0.6 and 0.7 for our composite membranes made by electroless plating. Fig. 10 shows the dependency of the hydrogen and nitrogen fluxes on the transmembrane partial pressure difference for a membrane with 7 μm thickness of the palladium layer and 400°C. These data originate from single-gas permeation experiments and from runs

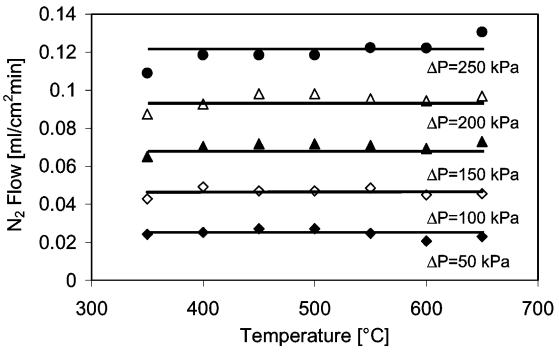

Fig. 9. Nitrogen flux through the same membrane as referred to in Fig. 8 under the same experimental conditions.

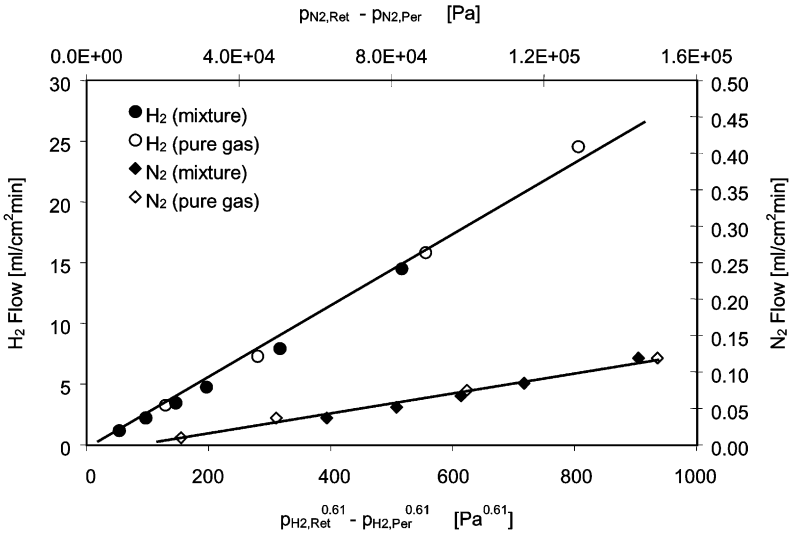

Fig. 10. Hydrogen and nitrogen fluxes through a 7 μm thick palladium–alumina membrane at 400°C vs. the driving force for the permeation. Single-gas hydrogen and nitrogen measurements and experiments with H_2/N_2 mixtures, in each case without sweep gas; increased retentate pressure and constant permeate pressure of 105 kPa; hydrogen flux is described by a pressure exponent of 0.61; nitrogen flux is proportional to the pressure difference.

with hydrogen–nitrogen mixtures. Both types of experiments were performed at ambient permeate pressure and elevated retentate pressure without a sweep gas. The points are well described by pressure exponents of 0.61 for hydrogen (determined by regression) and 1.0 for nitrogen.

The gentle deviation of the hydrogen pressure exponent from the theoretical value of 0.5 suggests that the hydrogen flux depends not exclusively on atomic diffusion through the palladium but is influenced to some extent by other processes, e.g. hydrogen adsorption on the palladium surface. It has been claimed that surface processes control the permeance of very thin palladium films [51], and for ultrathin palladium layers values of n close to 1.0 have been reported by different groups [49,58]. Table 2 provides a collection of literature results for various types of palladium composite membranes with different thicknesses. From this it appears that membranes thinner than 4–5 μm show a hydrogen pressure exponent near 1.0. Still no reliable limiting thickness can be given because the palladium layers have different morphologies and the flux data in most cases are analysed only graphically whether they comply with a prescribed pressure exponent of 0.5 or 1. On the other hand, if estimates for n are determined from measured fluxes by regression confidence in these estimates is limited because the experiments cover only a restricted range of the pressure difference, and the sensitivity of the flux to the pressure exponent is known to be weak [55].

The separation factor of a non-porous composite palladium membrane is defined as the ratio of the hydrogen flux to the flux of an inert species, e.g. nitrogen, at the same conditions. If the fluxes are based on permeation measurements with pure gases, the separation factor is referred to as *ideal*. The separation factors of our membranes determined from experiments in the permeation cell range from roughly 100 to over 1000. They decrease with increasing transmembrane pressure difference. This is reasonable because the nitrogen flow through leaks at the graphite seals or through remaining defects in the palladium film is more strongly affected by the pressure difference than the hydrogen flux through the palladium. The separation factors increase with higher temperature because the hydrogen flux rises with temperature, whereas the nitrogen flux is almost independent of temperature. However, the thickness of the palladium layer determines the effect of temperature on the separation factor. Layers thinner than about 6 μm undergo a

Table 2
Comparison of the permeation results of different palladium-based composite membranes[a]

Membrane	Preparation method	Thickness (μm)	Temperature (K)	Driving force ΔP (H_2) (kPa)	H_2-flux[b] (m^3/m^2 h)	Separation factor H_2/N_2	Pressure exponent	References
Pd-Ag/γ-Al_2O_3	SD	0.35	523	100	1.2–2.3	5.7	1.0	[48]
Pd/TiO_2	ELP-UV[c]	0.3–0.4	773	45	22.9	1140	1.0[e]	[59]
Pd-Ni/SS	VED	0.8	623–823	68	11.2–106.1	300–4700	1.0[e]	[49]
Pd/Al_2O_3	ELP-SG[d]	1.0	723	100	87	23	1.0[e]	[63]
Pd-Ru-In/SS	SD	1.5	645	100	4	Infinite	Not given	[64]
Pd-Ag/γ-Al_2O_3	SP	1.5–2.0	773	100	5.64	24	1.0	[50]
Pd/γ-Al_2O_3	CVD	0.5–5	573	100	0.81–1.62	200–300	Not given	[47]
Pd/Al_2O_3	CVD	4.4	573–873	100	>8.1	>1000	1.0[e]	[65–67]
Pd/Al_2O_3	CVD	∼5	673	199	29.8	240	0.5[e]	[68]
Pd-Ag/Al_2O_3	ELP	5.8	673	194	38.2	Infinite	0.5[e]	[69]
Pd/SS	ELP	6	673	100	4.7	Not given	0.5[e]	[70]
Pd/Al_2O_3	ELP/O	10	740	170	24.1	970	0.65	[57]
Pd/Al_2O_3	ELP/O	10	753	100	7.2	1000	0.5[e]	[71]
Pd/Al_2O_3	ELP	11.4	823	689	57.3	650	0.599–0.602	[72]
Pd/Al_2O_3	ELP	13	673, 773	200	11.9, 15.2	Infinite	Not given	[73]
Pd/Al_2O_3	ELP	7–15	673	100	7.0–10.8	100–1000	0.6–0.7	This work
Pd/SS	ELP	5	673	100	12.5	100–200	0.7	This work
Pd/SS	ELP	19–28	623	100	2–4	Up to 5000	0.434–0.646	[55]

[a] Pd-Ag: 23 wt.% Ag; SD: sputter deposition; ELP: electroless plating; VED: vacuum electro-deposition; CVD: chemical vapour deposition; SP: spray pyrolysis; O: osmotic pressure method.
[b] Photocatalytic activation.
[c] Activation by sol–gel process of a Pd(II)-modified boehmite sol.
[d] Estimated from cited references (at specified hydrogen partial pressure difference).
[e] Not determined by regression.

significant reduction of the separation factor at temperatures over 500°C [73]. These membranes showed lower hydrogen permselectivities during permeation measurements with binary mixtures of hydrogen with nitrogen compared to single-gas hydrogen measurements after a nitrogen test. In contrast membranes with palladium layers thicker than about 6 μm showed good thermal stability up to 650°C (cf. Figs. 8 and 9) and no difference in the hydrogen/nitrogen permselectivity when changing from pure gases to mixtures, as it can be seen in Fig. 10.

The hydrogen transport through a non-porous palladium film is an activated process. Under the assumption that the hydrogen pressure exponent does not depend on temperature the relationship between the hydrogen permeability and the temperature can be described by an Arrhenius law as follows:

$$Q = Q_0 \exp\left(-\frac{E_A}{RT}\right) \quad (4)$$

The measured hydrogen fluxes through a 15 μm thick palladium alumina membrane at different temperatures served to estimate the activation energy. Fig. 11 shows an Arrhenius plot of the hydrogen permeance against the reciprocal temperature. From this an apparent activation energy around 10 kJ/mol

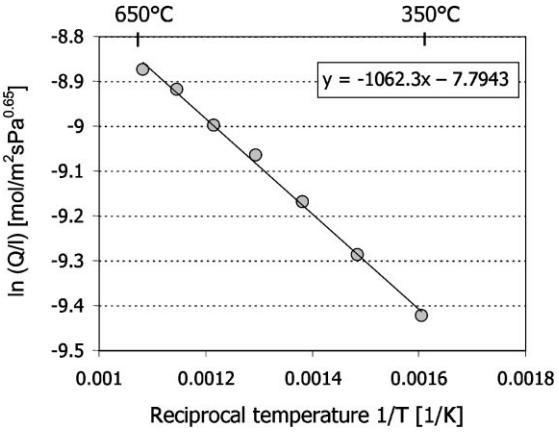

Fig. 11. Arrhenius plot of the hydrogen permeance of a palladium–alumina composite membrane; 15 μm thick palladium layer; temperature range: 350–650°C.

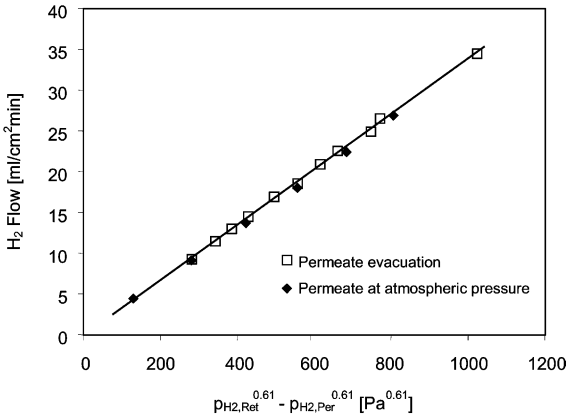

Fig. 12. Comparison of the hydrogen fluxes determined from measurements at reduced permeate pressure with measurements at increased retentate pressure; palladium–alumina membrane with a 7 μm thick palladium layer; temperature: 400°C.

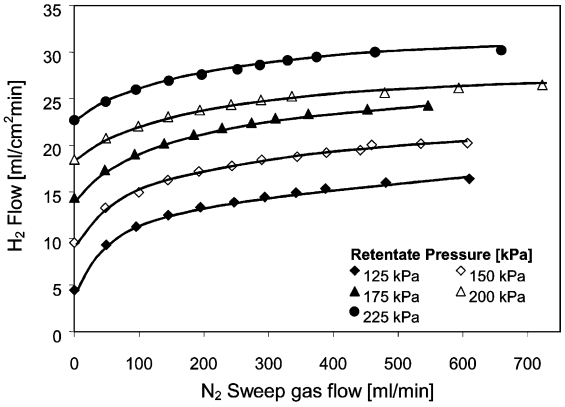

Fig. 13. Increase of the hydrogen flux through the use of a nitrogen sweep gas supplied on the support side of the membrane (cf. Fig. 4 for the design of the permeation cell). Influence of the transmembrane pressure difference on the sweep gas efficiency; palladium–alumina membrane with a 7 μm thick palladium layer; effective membrane area: 24 cm^2; temperature: 400°C; permeate pressure: 105 kPa.

was derived [73]. This value is in good agreement with those reported by other groups. For instance Weyten et al. [74] found 11–12 kJ/mol, Li et. al. [77] detected 12.3 kJ/mol, and Uemiya et al. [53] reported 10.7 kJ/mol for similar palladium composite membranes.

From Fig. 8 it can be seen that an increase of the retentate pressure leads to an increase of the hydrogen permeation rate. In cases where a high retentate pressure is unfavourable, e.g. for the dehydrogenation of hydrocarbons, a sufficient driving force for hydrogen permeation can be created by decreasing the permeate pressure. Fig. 12 compares the effect of these two methods on the hydrogen flux through a palladium–alumina membrane at 400°C. The experiments with permeate evacuation were performed at permeate pressures down to 25 kPa. No significant differences were observed, i.e. the results of both types of experiments fall together when plotting the hydrogen flux versus the driving force using the right hydrogen pressure exponent of 0.61.

The effect of a nitrogen sweep gas in the permeate compartment is shown in Fig. 13. The sweep gas reduces the partial pressure of hydrogen in the permeate and therefore increases the driving force for the permeation. The permeate pressure was kept constant at 105 kPa during these experiments, whereas the retentate pressure was varied from 125 to 225 kPa. The sweep gas efficiency is highest at the lowest pressure difference. For a retentate pressure of 125 kPa the hydrogen flux was raised by a factor of 3.7 at the highest nitrogen flow rate of 610 ml/min while it was increased only by 33% at 225 kPa (660 ml/min N_2). This can be attributed to the increased hydrogen flow through the membrane at higher pressure differences, which leads to a higher partial pressure of hydrogen at a given sweep gas flow rate. Note that the partial pressure of hydrogen in the permeate is not constant along the reactor when a sweep gas is used. It increases from zero at the entrance until to the highest value reached at the outlet. For example, at a retentate pressure of 125 kPa the hydrogen partial pressure in the permeate at the reactor outlet decreases from 105 kPa when no sweep gas is supplied to 41.4 kPa at the highest sweep gas flow rate of 610 ml/min. For the same sweep gas flow the hydrogen partial pressure in the permeate is reduced only to 57.2 kPa when the retentate pressure is set to 225 kPa. A second observation from Fig. 13 is that the slope of the curves levels off rather quickly with increasing sweep gas flow rate. Obviously for high sweep gas flow rates no real improvement of the hydrogen flux is observed even at high retentate pressures (i.e. high hydrogen flows) although the hydrogen partial pressure in the permeate is decreased substantially with increasing sweep gas flow. This behaviour is

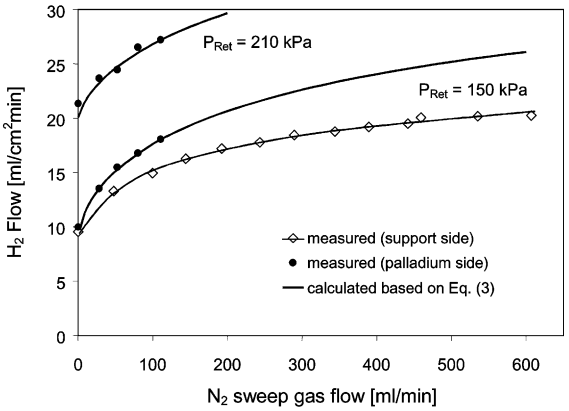

Fig. 14. Influence of the location of the sweep gas flow, i.e. at the support side or at the palladium side, on the efficiency of the sweep gas. Comparison of the measured hydrogen flows with the simulation results of a simple one-dimensional model employing Eq. (3) for description of the hydrogen permeation. Experimental conditions as of Fig. 13.

found only when the sweep gas is supplied on the support side of the membrane. It can be explained by the diffusion resistance of the support which leads to an increase of the hydrogen partial pressure in the pores of the support towards the surface of the palladium layer. In Fig. 14 the hydrogen fluxes obtained from experiments with the nitrogen sweep gas supplied on different sides of the membrane are compared. Clearly the sweep gas is more effective on the palladium side. Fig. 14 also shows the calculated hydrogen flux as a function of the sweep gas flow rate based on a simple one-dimensional plug-flow reactor model using Eq. (3) to describe the permeation of hydrogen. The agreement between the measurements and the simulation results is very good for the case where the sweep gas is supplied on the palladium side. In the opposite case the simple model overestimates the hydrogen flux, as it does not take into account the diffusion resistance of the support.

In a further experiment the membrane referred to in Fig. 10 was operated continuously at 400°C for about 1600 h, yet not at unchanged operating conditions. Fig. 15 shows the development of the hydrogen and nitrogen fluxes over time at an equal partial pressure difference of 45 kPa. Fig. 16 displays the separation factors. For each time reported several permeation experiments were carried out within short time to determine the partial pressure dependence of the fluxes, e.g. with different retentate pressures (pure gases) or with different hydrogen mole fractions in the retentate (H_2/N_2 mixtures). This allowed to convert the fluxes to a common driving force of 45 kPa for easy comparison.

During the first 220 h single-gas measurements with hydrogen followed by nitrogen and measurements with binary mixtures of hydrogen with nitrogen were carried out in an alternating fashion. Later on only measurements with pure hydrogen or binary mixtures were performed. The obtained hydrogen pressure exponents did not show any systematic changes over the whole duration of the experiment but only random fluctuations between 0.6 and 0.7. Still the hydrogen flux curves from the two types of measurements do not fall together, in particular not during the initial phase ($t < 400$ h). Despite these differences in the hydrogen flux the nitrogen fluxes from both methods are in good agreement from the beginning on, which means that no pinholes were formed and the measured effects are related to the intact palladium layer. Again the moderate separation factors of 80–140 (binary mixtures) evident from Fig. 16 are caused by a certain leakage at the graphite seals.

The hydrogen flux of the fresh membrane was 3.5 ml/cm^2 min. This value was found with pure hydrogen and with a hydrogen–nitrogen mixture. In the initial phase the hydrogen flux increased with time pointing to structural changes of the palladium layer, e.g. a change of the grain size or a compaction of the layer. Note that no temperature treatment had been applied to the membranes before the experiment. This increase is witnessed both by the single-gas results and by the mixture data, but in the single-gas experiments higher hydrogen flows were detected compared to the experiments with mixtures. So far no indubitable explanation can be given for this behaviour. It is assumed that a change of the atmosphere from pure hydrogen to pure nitrogen, that comes along with a complete release of the hydrogen dissolved in the metal, leads to a temporary increase of the hydrogen permeability of the palladium layer caused by a modification of its surface or its grain structure. This is based on the observation that the first measurement of the hydrogen flux after a nitrogen test always showed a distinctly higher hydrogen flow even though the nitrogen flow before was unchanged. In the sequel the

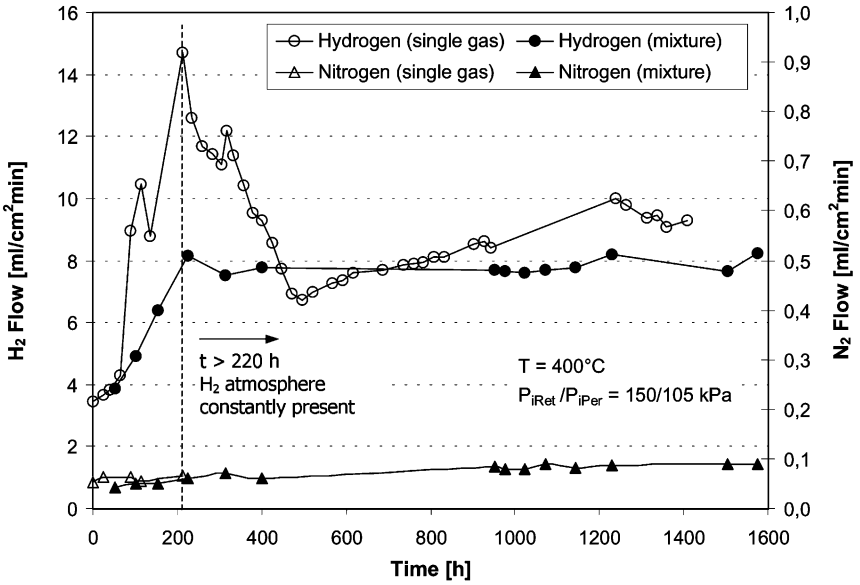

Fig. 15. Hydrogen and nitrogen flows through a palladium–alumina composite membrane with 7 μm thickness of the palladium layer at 400°C as a function of time; retentate pressure: 150 kPa; permeate pressure: 105 kPa; single-gas (H_2 or N_2) and binary mixture (H_2 and N_2) permeation experiments without sweep gas.

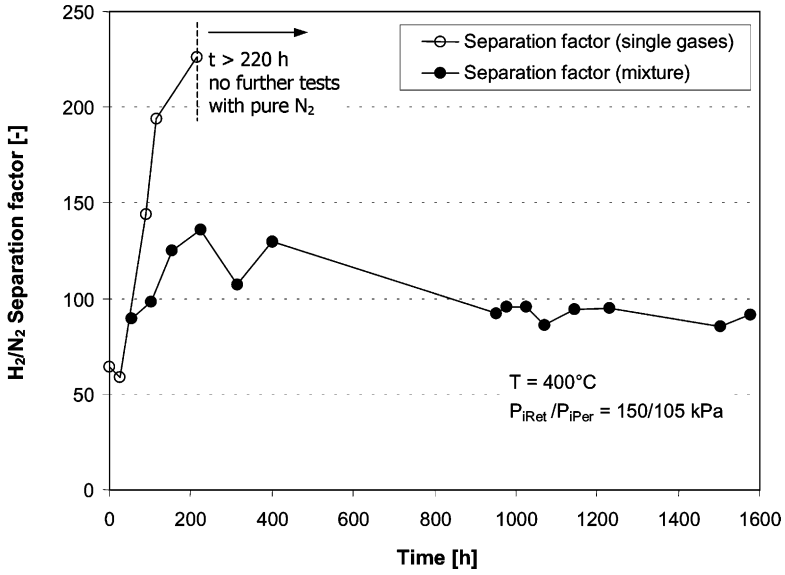

Fig. 16. Hydrogen–nitrogen separation factors of the palladium–alumina composite membrane referred to in Fig. 15 as a function of time.

hydrogen flow returned. Yet the interpretation of this effect suffers from the superimposed increase of the hydrogen flux with time. After two cycles ($t > 220$ h) no further single-gas nitrogen tests were performed and the membrane was kept constantly in contact with a hydrogen containing atmosphere. This brought the single-gas hydrogen flow slowly down from the peak value of 14.7 to about 8 ml/cm^2 min, which was the stationary level detected in the experiments with binary mixtures. The question why the hydrogen flux measured with pure hydrogen needed about 200 h to return to the same level as found in the experiments with hydrogen/nitrogen mixtures remains open just as the question why it slowly increased again after passing a minimum at about 450 h. Further studies on the supposed structural changes of the palladium layer are necessary to elucidate the reasons for this behaviour.

2.4.3. Comparison of the permeation results with published data

A comparison of the permeation results of the membranes prepared in this work with published data of similar membranes at a first glance reveals many similarities (flux, separation factor and apparent activation energy). However, a large scattering of the published data becomes evident when trying to evaluate all results on a common basis, i.e. as a function of the thickness of the metal layer and for a given temperature and a given hydrogen partial pressure difference. This holds even when focusing solely on pure palladium membranes with high H_2/N_2 separation factors. Fig. 17 shows a plot of the hydrogen flux at 400°C versus the thickness of the palladium layer for composite palladium membranes reported by different groups. The data were taken from various tables and figures in the original papers [53,55,57,59,64–77]. In some cases it was necessary to convert the fluxes to the common hydrogen partial pressure difference of 100 kPa to enable a direct comparison. If so this was done employing the hydrogen pressure exponents given by the authors. The solid lines represent calculations for self-supporting palladium foils relating the flux to the inverse thickness of the palladium. These lines mark the behaviour expected when the diffusion of hydrogen atoms controls the permeation rate. Sorption effects and the diffusion resistance of the boundary layers are ignored. Three different sources [78–80], each based on measurements with

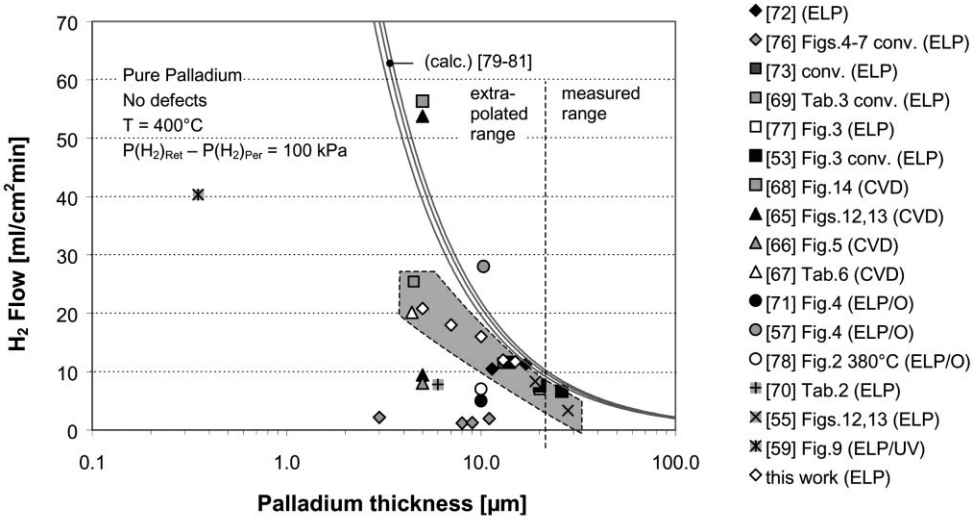

ELP = Electroless plating; ELP/O = ELP combined with osmosis; ELP/UV = ELP with UV-based activation; CVD = Chemical vapour deposition; conv. = converted to 100 kPa hydrogen partial pressure difference; curves adapted from [79-81]

Fig. 17. Hydrogen flow through palladium composite membranes reported by different groups for 400°C and 100 kPa partial pressure difference. Comparison with extrapolated hydrogen flows through self-supporting palladium foils.

foils of 50 μm thickness or higher, were used which obviously show good agreement.

The first observation is that the hydrogen fluxes determined with supported palladium layers mainly fall below the theoretical line of the self-supporting palladium foils, although a few membranes have shown higher values. The majority of the data points lies in the shaded region in Fig. 17. The hydrogen fluxes of membranes with palladium layers above 12 μm thickness show rather good conformity. These membranes have been all made by electroless plating. The deviation increases as the palladium thickness is decreased. Hughes and co-workers reported hydrogen fluxes for supported palladium layers prepared by electroless plating (osmotic pressure method) ranging from 5 to 28 ml/cm^2 min (cf. Fig. 17, circles) [57,70,69]. Even more pronounced are the differences described by Morooka and co-workers [64–66]. They reported hydrogen fluxes ranging from 8 to 54 ml/cm^2 min for palladium layers with approximately 5 μm thickness prepared by CVD (cf. Fig. 17, triangles). Very low hydrogen fluxes have been reported by Paglieri et al. [75] for palladium layers below 12 μm thickness which have been deposited by electroless plating, although in a previous publication higher values were reported for membranes with even thicker palladium layers (cf. Fig. 17, rhombuses) [71].

A number of factors may be responsible for the deviating results. Some errors are certainly associated with the fact that the membranes have been used not exactly under the same experimental conditions and that the data have been read in part from figures or were converted to a common partial pressure difference. Another important factor is the difficulty to determine the true thickness of the palladium layers, e.g. by weight increase of the membranes after palladium deposition or by measuring the thickness from SEM micrographs taken at different locations. Particular problems occur when the palladium penetrates into the pores of the support, or when the deposition on the surface is not homogeneous. Besides, the palladium layers deposited by electroless plating and CVD are less compact than palladium foils produced by metallurgical techniques like cold rolling and have a different microstructure. It can be expected that the microstructure is linked to the permeability. Impurities introduced with the chemicals used or decomposition products formed during the preparation (carbon) can also change the permeability. In the preparation by CVD a filling up of the support pores with small-sized palladium particles starting from the pore walls takes place as opposed to the growth of a connected film on top of the surface in electroless plating. It has been reported that the hydrogen transport through palladium composite membranes made by CVD is not governed by the usual solution-diffusion mechanism. To explain this some authors have claimed that hydrogen diffuses along narrow pores whose walls are covered with palladium [64–66]. Others assumed a short-range solution-diffusion transport through individual palladium grains interrupted by molecular diffusion across the intergranular volume [47]. A linear dependence of the hydrogen flux on the partial pressure difference was found for CVD-type palladium composite membranes with metal thicknesses around 5 μm, whereas definitely lower hydrogen pressure exponents were detected for electroless plated membranes with palladium layers of similar thickness. The hydrogen fluxes through most CVD-type membranes are lower than expected in view of the palladium thickness [62,81]. Together with the observed increase of the hydrogen flux with increasing palladium grain size [47] this seems to backup the supposed transport mechanism.

Some of the best permeation results so far have been obtained with a modified electroless plating where the activation of the surface was achieved by photocatalysed deposition of palladium on a TiO_2 membrane [59]. After the plating a coherent palladium film of 0.3–0.4 μm thickness was obtained which showed a hydrogen flux of 40 ml/cm^2 min at 400°C and a hydrogen partial pressure difference of 100 kPa. This membrane had a hydrogen pressure exponent close to 1 indicating that surface processes control the hydrogen flux.

What is not discussed in most publications is the change of the permeation properties with time and with changing gas atmospheres. From Fig. 15 we read hydrogen fluxes ranging from 3.5 to 14.7 ml/cm^2 min for the same membrane depending on the history of the measurement. The stationary hydrogen flux of this membrane was between 8 and 10 ml/cm^2 min and was obtained not before some hundred hours of operation. Note that at any time of the experiment the hydrogen partial pressure exponents determined from measurements with different hydrogen pressures were in the

same range (0.6–0.7) and no change of the nitrogen flux was detected.

One must conclude that the available experimental data do not allow to assess the maximum hydrogen flux through an ultrathin composite palladium membrane. It is not clear yet at which palladium thickness surface processes actually begin to control the permeance, and no detailed information is available on the influence of the microstructure of differently produced palladium layers on the hydrogen permeance and the permselectivity.

The transition from atomic diffusion control to a control by surface effects depending on the thickness of the palladium layer can be analysed using a rather simple model. It has been said that the permeation of hydrogen through a palladium membrane is a sequence of several steps. If one ignores the diffusion resistance of the support and of possible boundary layers the first step is the adsorption of hydrogen which is accompanied by a dissociation:

$$H_2 + 2[\,] \Leftrightarrow 2[H] \tag{5}$$

The adsorption is reversible, hence the net rate can be expressed by the difference between the adsorption and desorption rates as follows:

$$\bar{r} = k_a p_{H_2} \theta^2 - k_d \theta_H^2 \tag{6}$$

The next step is the entry of hydrogen atoms into the palladium lattice. In the most simple concept hydrogen can enter the palladium lattice at any of the adsorption sites. Although in reality a lateral displacement may be necessary because the entry occurs only at specific positions in the lattice [82] we prefer here the most simple case. Moreover, we assume that the transference of hydrogen into the lattice is fast compared to the subsequent diffusion. Under these conditions the flux can be written alternatively to Eq. (3) in terms of the surface coverage of hydrogen as follows:

$$J = \frac{Q^*}{l}(\theta_{HR} - \theta_{HP}) \tag{7}$$

where J denotes the hydrogen flux, Q^* the permeability coefficient and l is the thickness of the palladium layer.

The third step is the release of hydrogen atoms from the lattice to the surface, and the fourth step is the recombination and desorption of hydrogen to the permeate. These two can be summarised and treated the same way as steps 1 and 2, again provided that the release of hydrogen atoms from the lattice occurs much faster than the atomic diffusion.

We assume further that on either surface of the membrane we have the same number of adsorption sites per unit area, that is the same values of k_a and k_d hold for the retentate and permeate sides. The hydrogen balance for the palladium surface at the retentate side reads

$$k_a p_{HR} \theta_R^2 = k_d \theta_{HR}^2 + \frac{Q^*}{l}(\theta_{HR} - \theta_{HP}) \tag{8}$$

whereas on the palladium surface at the permeate side we have

$$\frac{Q^*}{l}(\theta_{HR} - \theta_{HP}) + k_a p_{HP} \theta_P^2 = k_d \theta_{HP}^2 \tag{9}$$

If no other species are adsorbed on the palladium surface except hydrogen we can write a very simple balance for the surface coverage as follows:

$$\theta_{HR} + \theta_R = 1, \qquad \theta_{HP} + \theta_P = 1 \tag{10}$$

Combining Eq. (10) with Eqs. (8) and (9) yields two non-linear equations for the unknown surface coverages θ_{HR} and θ_{HP} which can be solved numerically for given values of the adsorption and desorption rate constants k_a and k_d and the permeability coefficient Q^* if the partial pressure of hydrogen in the retentate and permeate and the thickness of the palladium layer is known (cf. Eq. (11)).

$$\theta_{HR} = \theta_{HP} + \frac{l}{Q^*}[k_d \theta_{HP}^2 - k_a p_{HP}(1 - \theta_{HP})^2],$$
$$\theta_{HP} = \theta_{HR} + \frac{l}{Q^*}[k_d \theta_{HR}^2 - k_a p_{HR}(1 - \theta_{HR})^2] \tag{11}$$

This model was used to analyse the permeation data of our composite palladium membranes (only pure Pd) having palladium thicknesses between 5 and 15 μm. The idea was that the measured partial pressure dependence of the hydrogen flux reflects the combined influences of the atomic diffusion through the palladium layer and the adsorption/desorption on the palladium surface. Hence, it should be possible to determine a set of estimates for k_a, k_d and Q^* which can account for the permeation behaviour of the membranes and provides a basis for an estimation of the influence of the palladium thickness on the hydrogen flux.

A weighted least squares objective function was defined based on the measured and calculated hydrogen fluxes through the membrane as follows:

$$\mathrm{SS} = \frac{1}{n_\mathrm{m}} \sum_d \sum_i \frac{1}{n_\mathrm{d}} \left(\frac{J_\mathrm{exp} - J(k_\mathrm{a}, k_\mathrm{d}, Q^*)}{J_\mathrm{exp}} \right)^2 \quad (12)$$

Data from 36 permeation measurements with electroless plated palladium membranes of different palladium thickness (5, 7, 10, 13 and 15 μm) were evaluated. All measurements were made at 400°C. One additional dataset from measurements with a 70 μm thick palladium layer (prepared by thermal spraying [61]) at the same temperature was added to secure that the model is able to reproduce the permeation behaviour of thick palladium layers. The weighting factor $1/n_\mathrm{d}$ in Eq. (12) ensures that each group of data related to a certain membrane thickness contributes equally to the objective function. n_d denotes the number of experiments carried out with a membrane of thickness d, whereas n_m is the number of membranes (i.e. different thicknesses). The deviation between measured and calculated fluxes is scaled with the measured fluxes, which means that the measurement error is supposed to be proportional to the measured flux.

The data were analysed by calculating and plotting the objective function versus the three parameters k_a, k_d, and Q^*. No regression method was used because a correlation was detected among the parameters k_d and Q^*. For given values of k_d parameter estimates for k_a and Q^* were successively determined. Fig. 18 shows the estimates of k_a and Q^* as a function of k_d. From this it is obvious that a square-root dependence between the optimal values for Q^* and k_d exists while no such correlation is effective between k_a and k_d. The residual objective function does not vary much with changing k_d. Only a weak minimum exists close to $k_\mathrm{d} = 10^5$ mol/m^2 s with $Q^* = 1.38 \times 10^{-3}$ mol m/m^2 s and $k_\mathrm{a} = 8 \times 10^{-6}$ mol/m^2 s Pa. Fig. 19 shows a

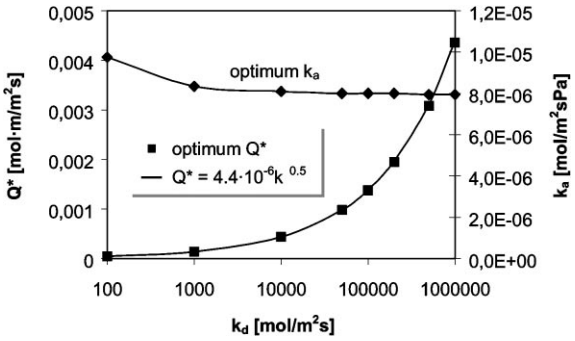

Fig. 18. Correlation between the optimal estimates for the parameters of the permeation model Q^*, k_a and k_d (cf. Eqs. (6)–(11)).

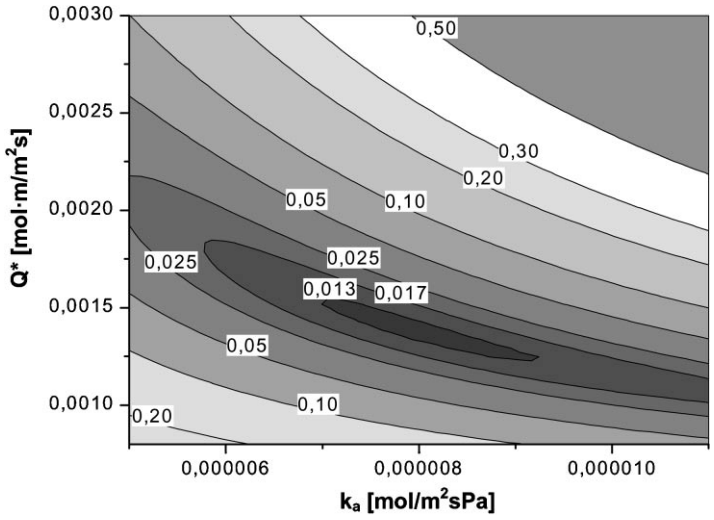

Fig. 19. Contour plot of the objective function according to Eq. (12) for variation of the parameters Q^* and k_a (k_d fixed at the optimal value of 10^5 mol/m^2 s).

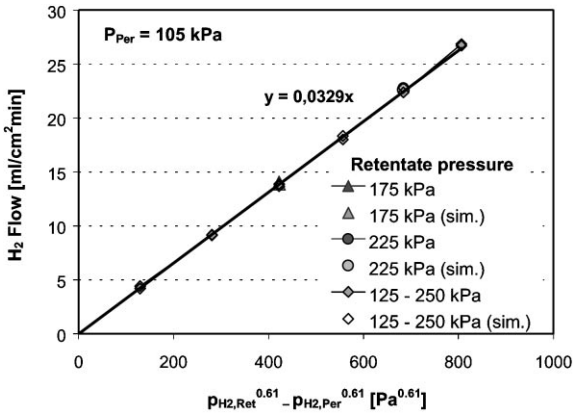

Fig. 20. Comparison of calculated and measured hydrogen flows through a palladium–alumina composite membrane with 7 μm thickness of the palladium layer at 400°C as a function of the driving force for the permeation; measurements with pure hydrogen; constant permeate pressure of 105 kPa and varying retentate pressure (sim. denotes calculated hydrogen flows).

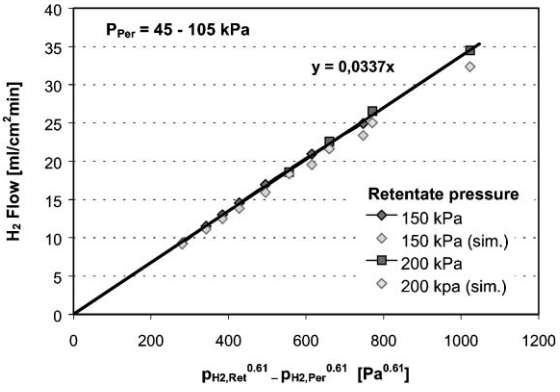

Fig. 21. Comparison of calculated and measured hydrogen flows through a palladium–alumina composite membrane with 7 μm thickness of the palladium layer at 400°C as a function of the driving force for the permeation; measurements with pure hydrogen; permeate evacuation at different retentate pressure levels (sim. denotes calculated hydrogen flows).

contour plot for the parameters k_a and Q^* near the optimum which reveals a fair accuracy of the estimation of these parameters for fixed k_d. The residual value of the objective function is around 0.01215. This corresponds to an average deviation of 11% between the measured and calculated hydrogen fluxes (related to the measured values).

The model can describe the measured partial pressure dependence of the hydrogen flux quite well. This is evident from the Figs. 20 and 21 which show the data for a membrane with 7 μm palladium thickness. Besides it can reproduce the increase of the hydrogen flux with reduced palladium thickness, as it is shown in Fig. 22. The model predicts that the hydrogen flux could reach up to 0.4 mol/m^2 s for very thin palladium layers, which then is controlled by the kinetics of the surface processes. At high palladium thicknesses the predicted hydrogen fluxes coincide with the values obtained for palladium foils, reported for example by Itoh et al. [78]. The predicted hydrogen flux for palladium thicknesses in the sub-micron range is slightly higher than the flux measured by Wu et al. [59]. However, in view of the fact that the model is extrapolated and that the transport resistance of the support may already have some influence in this range the prediction seems to be reasonable. This holds also for the change of the hydrogen pressure exponent with changing palladium thickness, which is shown in Fig. 23. Note that the hydrogen pressure exponent n is defined in relation to Eq. (3), whereas the model represented by Eqs. (6)–(11) has no such parameter. The curves in Fig. 23 were obtained by evaluating simulation results from Eqs. (6)–(11) with the simplified Eq. (3). One dataset refers to constant hydrogen pressure in the retentate and changing permeate pressure (upper curve) and the other vice versa (lower curve). The deviation between the two datasets shows

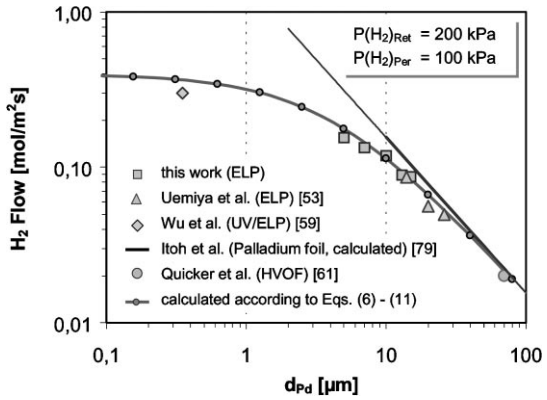

Fig. 22. Hydrogen flow through palladium composite membranes at 400°C as a function of the palladium thickness. Permeation of pure hydrogen at a retentate pressure of 200 kPa and a permeate pressure of 100 kPa. Comparison of simulation results with measured data.

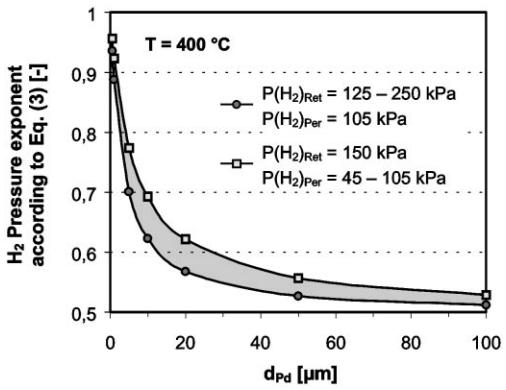

Fig. 23. Variation of the hydrogen pressure exponent with the thickness of the palladium layer for different measurement conditions. Obtained by evaluation of simulation results from Eqs. (6)–(11) with the simplified Eq. (3).

that the model predicts a difference in the hydrogen pressure exponent depending on the hydrogen pressure. Low hydrogen pressures (permeate evacuation) give higher values of n compared to high hydrogen pressures (increased retentate pressure). Our membranes have thicknesses in the range of 5–15 μm. In this range the predicted hydrogen pressure exponent varies between 0.6 and 0.7, as it was found also in the experiments.

2.4.4. Kinetic compatibility of hydrogen generation and hydrogen removal

The performance of a packed-bed membrane reactor depends not only on the permeation behaviour of the membranes employed. The basic requirement for a significant increase of the overall reaction rate is that the generation of the product which is to be withdrawn by the membrane must occur at a rate comparable to the permeation rate. More precisely, the amount of product generated in a given volume of the packed-bed per unit time must match the amount of product permeating per unit time through the membrane area enclosing this volume at the existing transmembrane partial pressure difference. The two numbers to be compared here are the volume-based rate of hydrogen formation and the volume-based rate of hydrogen permeation, as described in Eq. (13).

$$\rho_b R_{H_2,Cat} \approx a_V \frac{Q_{H_2}}{l}(p_{HR}^n - p_{HP}^n) \quad (13)$$

The former is the product of the effective hydrogen generation rate per unit weight of catalyst with the packed-bed density. The latter is the hydrogen permeance of the membrane multiplied with the driving force for the permeation multiplied with the membrane area per unit volume. Neither the left side nor the right side of Eq. (13) are constant within the reaction volume. The reaction rate is influenced by the temperature and by the concentration of the reactants. Hence, it varies along the reactor axis, and if radial gradients are present, also in radial direction. If heat or mass transfer limitations from the gas phase to the catalyst pellets or inside the pellets exist, then the reaction rate varies also within the catalyst. The hydrogen flux across the membrane is affected by the temperature and by the partial pressure difference of hydrogen which changes along the reactor axis likewise. A quantitative assessment would require a thorough reactor simulation considering the kinetics of all relevant processes, which is not the intention of this paper. Yet a quick analysis of the kinetic compatibility of reaction and permeation is attempted by inserting appropriate average values for the quantities in Eq. (13). Table 3 shows the results for two common dehydrogenation reactions which we have studied experimentally. The hydrogen generation rates were determined from kinetic experiments in lab-scale packed-bed reactors operated at conversions well below the equilibrium level.

The first example is the dehydrogenation of ethylbenzene to styrene on a commercial iron oxide catalyst. The crucial factors of this process are the high dilution of the ethylbenzene feed with steam which is necessary among other things to prevent carbon deposition and the low pressure which is applied to reach a high conversion. Both factors are responsible for the low reaction rate and the small driving force for the hydrogen permeation. The maximum partial pressure of hydrogen in the retentate given in Table 3 corresponds to the equilibrium composition for the specified reference conditions. The maximum hydrogen flux was calculated based on the assumption that this value is reached in the retentate, whereas in the permeate the hydrogen partial pressure is close to zero. The true (average) driving force is lower, but as a first approximation it is instructive to use this best case scenario for estimating the minimum membrane area required. The experimentally determined hydrogen generation rate depends on the particle size of the catalyst.

Table 3
Comparison of the hydrogen generation and removal rates for common dehydrogenation reactions in a packed-bed membrane reactor

Reaction	Ethylbenzene dehydrogenation	Propane dehydrogenation
Catalyst	K_2CO_3/Fe_2O_3 (Süd-Chemie)	Cr_2O_3/Al_2O_3 (Linde)
Packed-bed density (kg/m^3)	1200	1225
Pellet shape and size (diameter × length)	Cylindrical: 3 mm × 3–4 mm (crushed: 0.8–1.0 mm)	Cylindrical: 4.8 mm × 4.8 mm (crushed: 0.5–0.63 mm)
Reference conditions		
Temperature/pressure	600°C/100 kPa	580°C/130 kPa
Feed composition (mol/mol)	EB/H_2O = 8/92	C_3H_8/H_2 = 80/20
Equilibrium conversion	X_{eq} = 0.79	X_{eq} = 0.30
H_2 generation rate at reference conditions (mean value in a packed-bed without H_2 removal)	1.9 (3.5) mol/m^3 s, WHSV ≈ 0.78–0.91 h^{-1}, X_{EB} ≈ 0.60–0.64	11.0 (31.7) mol/m^3 s, GHSV ≈ 11100 h^{-1}, $X_{Propane}$ ≈ 0.08–0.23
Maximum H_2 partial pressure in the retentate at reference conditions (equilibrium value) (kPa)	5.7	46.3
Maximum H_2 flux through a 15 μm thick palladium layer at reference conditions (calculated from Eqs. (6)–(11) for $p_{HR} \approx 0$) (mol/m^2 s)	2.27×10^{-2}	1.12×10^{-1}
Required membrane area per unit volume to match H_2 formation rate (m^{-1})	83.7 (154.2)	98.2 (283.0)
Required tube diameter (multitubular module) to match H_2 formation rate (mm)	47.8 (25.9)	40.7 (14.1)
Comments/challenge	High dilution by steam and low pressure cause low reaction rate and small driving force for H_2 permeation	Reaction rate decreases quickly due to carbon deposition (within hours) Hydrogen removal could accelerate carbon deposition

Conventional extruded pellets with 3 mm diameter show a reduced reaction rate compared to fine catalyst particles obtained by crushing of the original pellets (values in parenthesis). Obviously pore diffusion limitation leads to concentration gradients inside the pellets which lower the reaction rate. The calculation according to Eq. (13) reveals that depending on the particle size of the catalyst minimum membrane areas between 83.7 and 154.2 m^{-1} would be needed. If one assumes a tubular geometry where the membrane and the catalyst are both placed on the tube side, this would be equivalent to a maximum inner diameter of the tubes of 47.8 or 25.9 mm, respectively. If a kinetic model [83] is used to predict the rate of hydrogen generation for the conditions at the reactor entrance, that is at zero conversion, one obtains a value around 6 mol/m^3 s. This is the theoretical maximum of the hydrogen formation rate of the catalyst. It would require a membrane area of 264 m^{-1} or a tube diameter of 15.1 mm, respectively.

The second example shown in Table 3 is the dehydrogenation of propane to propylene on a chromia-based catalyst. Compared to ethylbenzene dehydrogenation the hydrogen generation rate per unit volume is much higher, and so the differences between the reaction rates obtained with pellets and fine particles are more pronounced. The reaction rate is higher mainly because the feed is not diluted with an excess of steam but only with about 20% hydrogen to control the carbon deposition rate. This leads to a reasonable driving force for hydrogen permeation but also to a low equilibrium conversion, which in turn increases the potential benefit of the membrane reactor. However, due to the carbon deposition the activity of the catalyst decreases gradually, which makes a cyclic operation necessary. After several hours on stream the catalyst must be re-oxidised with air to restore its activity. Since in the commercial process hydrogen is added to the feed to extend the dehydrogenation time, it is feared that in the membrane reactor the

activity might deteriorate more quickly when a large fraction of the produced hydrogen is removed from the packed-bed. The required membrane area is larger than for ethylbenzene dehydrogenation although the difference is not so pronounced as suggested by the difference of the reaction rates because the driving force for the permeation is higher likewise. For the pellet catalyst a tube diameter of 40.7 mm would be the highest, whereas for the crushed catalyst a tube diameter below 14.1 mm is needed. The theoretical maximum of the hydrogen generation rate for the listed reference conditions determined from the kinetic model is about 46 mol/m^3 s and would require a membrane area of 412 m^{-1} or a tube diameter of 9.7 mm, respectively. These estimates refer to the initial activity. However, the activity decreases with time so that the cycle-averaged reaction rates are lower than the values given in Table 3. Therefore, larger tube diameters might be effective as well.

In both examples significant differences occur between the catalytic activity of pellets and crushed particles demonstrating the impact of pore diffusion limitation on the performance of the catalysts. The hydrogen generation rate could be increased by decreasing the diffusion resistance, i.e. reducing the catalyst dimensions, but under the high throughput conditions of industrial packed-bed reactors this would cause a prohibitive pressure drop. One concept that might be interesting then is to coat the catalyst directly on the membrane, i.e. on the opposite side of the palladium layer, as it is indicated in Fig. 24. A rough estimate of the necessary thickness of the catalytic layer can be derived from the reciprocal of the minimum membrane area in Table 3 which gives the catalyst volume per unit (membrane) area. This must be multiplied with the factor $1 - e_b$ because the rate of hydrogen generation is based on the overall packed-bed volume including the voidage, while a catalyst layer on the membrane is equivalent to a flat plate with a density comparable to a normal pellet. If we consider the maximum reaction rate calculated from the kinetic models we obtain a thickness of the catalytic layer of 1.9 mm for ethylbenzene dehydrogenation and of 1.2 mm for propane dehydrogenation. Since this falls into the range of the support thickness of the composite membrane one option could be to integrate the dehydrogenation catalyst directly into the membrane support to give a structured membrane catalyst.

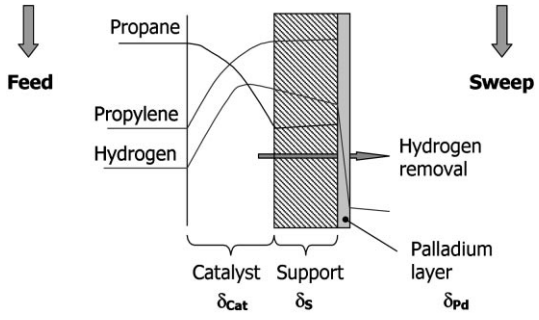

Fig. 24. Basic principle of a palladium composite membrane with built-in dehydrogenation catalyst. Qualitative shape of the concentration profiles of the reactants over the composite membrane. The catalyst may be applied in the form of a separate layer, as it is shown here, or be integrated in the membrane support.

An additional advantage of a thin catalyst layer on the adjacent side of the membrane could be an improved temperature control. The dehydrogenation consumes a large amount of heat. In a tubular packed-bed of a few centimetres diameter a temperature decrease by 10–30 K from the wall to the centre is not unusual and may lead to a significant reduction of the reaction rate. This can be avoided if the permeated hydrogen is burned on the shell side of the membrane and the heat of the reaction is transported via heat conduction over relatively short distance to the catalytic reaction zone in the membrane support. Yet so far no sufficient experimental results are available which would allow to judge the potential of such a concept for real applications.

2.4.4.1. Influence of the reaction rate law. Besides the magnitude of the hydrogen generation rate their dependence on the partial pressure of the reactants can have ready additional hurdles. Hydrocarbon dehydrogenations are endothermic reactions which are associated with a volume increase according to the general stoichiometry:

$$C_mH_{n+2} \underset{k^-}{\overset{k^+}{\rightleftarrows}} C_mH_n + H_2, \quad \Delta H_R > 0 \tag{14}$$

Hence, the equilibrium conversion increases towards higher temperature and lower pressure. If one ignores undesired side reactions the overall dehydrogenation rate can be described in many cases by the rate law

given in Eq. (15), which considers that the unsaturated product is more strongly adsorbed on the catalyst than the hydrocarbon feedstock. This was confirmed also for ethylbenzene dehydrogenation and propane dehydrogenation.

$$r = \frac{k(p_{C_mH_{n+2}} - (p_{C_mH_n} p_{H_2}/K_p))}{(1 + K_{C_mH_n} p_{C_mH_n})^q},$$

$$K_p = \left.\frac{p_{C_mH_n} p_{H_2}}{p_{C_mH_{n+2}}}\right|_{eq} \tag{15}$$

where k is the rate constant, K_p the equilibrium constant of the reaction, and $K_{C_mH_n}$ is the adsorption equilibrium constant of the unsaturated product. All three are a function of the temperature. While the rate constant and the equilibrium constant both increase with higher temperature, the adsorption equilibrium constant decreases as a matter of the reduced surface coverage. The exponent q of the adsorption term in the denominator is normally equal to 1 or 2, depending on the number of surface sites involved in the rate controlling step.

It is obvious from Eq. (15) that the drop of the reaction rate to zero upon approaching the equilibrium composition can be prevented in a membrane reactor by withdrawal of the produced hydrogen from the catalyst. Theoretically, if the entire hydrogen could be removed, the reverse reaction would be completely blocked. However, depending on the value of $K_{C_mH_n}$ the beneficial effect of hydrogen removal on the reaction rate can be counteracted with increasing conversion by a growing inhibition of the reaction rate due to adsorption of the unsaturated product. Fig. 25 illustrates this influence for the simple case of an ideal plug-flow membrane reactor working at constant temperature. It is based on the general form of the design equation of a plug-flow reactor, valid for arbitrary kinetics:

$$\frac{V_R}{\dot{n}^0_{C_mH_{n+2}}} = \frac{\tau}{c^0_{C_mH_{n+2}}} = \int_0^{X^e} \frac{dX}{r} \tag{16}$$

which relates the quotient of the reactor volume divided by the molar feed flow rate to the conversion X. The conversion is defined as follows:

$$X = 1 - \frac{\dot{n}_{C_mH_{n+2}}}{\dot{n}^0_{C_mH_{n+2}}} \tag{17}$$

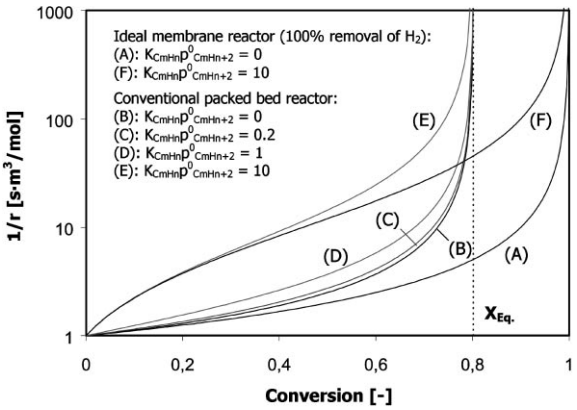

Fig. 25. Reciprocal reaction rate in an ideal plug-flow packed-bed reactor (conventional or membrane reactor) as a function of the conversion of the hydrocarbon feed. Influence of the removal of hydrogen on the reaction rate for different values of the adsorption inhibition parameter $K_{C_mH_n} p^0_{C_mH_{n+2}}$. Reaction rate according to Eq. (15) with $q = 1$, $K_p = 30\,\text{kPa}$, $p^0_{C_mH_{n+2}} = 10\,\text{kPa}$ and $k = 10^{-4}\,\text{mol/m}^3\,\text{s Pa}$.

According to Eq. (16) the reciprocal of the reaction rate is plotted as a function of the conversion for different limiting cases of the rate law given in Eq. (15). The exponent q was set to 1 for these calculations. The other parameters are $K_p = 30\,\text{kPa}$ and $p^0_{C_mH_{n+2}} = 10\,\text{kPa}$. The rate constant k was fixed arbitrarily to $10^{-4}\,\text{mol/m}^3\,\text{s Pa}$ to give an initial rate at zero conversion of $1\,\text{mol/m}^3\,\text{s}$. The area below the curves in Fig. 25 represents the integral on the right side of Eq. (16). It is a direct measure of the residence time needed for a desired conversion at a given feed concentration.

Curve (A) denotes the hypothetical case of entire removal of the produced hydrogen in a packed-bed membrane reactor and no adsorption of the unsaturated hydrocarbon, i.e. $p_{H_2} = 0$ and $K_{C_nH_m} = 0$. The reverse reaction is completely blocked, and so full conversion can be achieved. The reaction rate decreases linearly with increasing conversion. This is the optimum with respect to a high reaction rate, i.e. a low amount of catalyst required. Curve (B) shows the same situation but without removal of hydrogen, as it would occur in a conventional packed-bed reactor. The reaction is reversible and hence it cannot surpass the equilibrium conversion, which is about 0.8 in this example. Curve (B) is always above curve (A).

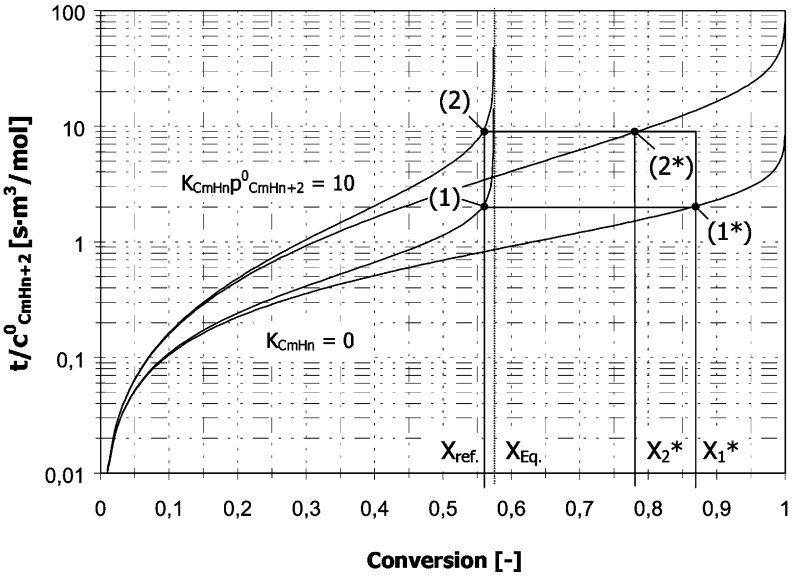

Fig. 26. Influence of the preferred adsorption of the unsaturated product C_nH_m on the performance of an ideal plug-flow packed-bed membrane reactor. Kinetic parameters as of Fig. 25; $p^0_{C_mH_{n+2}} = 50\,\text{kPa}$; curves (1/1*) correspond to curves (B/A), curves (2/2*) to curves (E/F) in Fig. 25.

This reflects the lower space time yield of the conventional packed-bed reactor compared to the ideal membrane reactor. The gap between the two curves becomes larger with shrinking distance to the equilibrium conversion because the conventional reactor then suffers from the growing rate of the reverse reaction.

Curves (C)–(E) also stand for the reaction in the conventional packed-bed reactor but with inhibition by adsorption of the target product C_mH_n. The value of the product $K_{C_mH_n} p^0_{C_mH_{n+2}}$ specifies the extent of this inhibition. It gives the maximum increase of the denominator in Eq. (15) for the hypothetical case that the partial pressure of the product would reach the initial partial pressure of the hydrocarbon feed component. A value of 0.2 for this parameter was used for calculation of curve (C). This marks a reduction of the reaction rate due to product adsorption not exceeding 20%. Curve (D) shows the situation for $K_{C_mH_n} p^0_{C_mH_{n+2}} = 1.0$, that is halving of the reaction rate. Curve (E) stands for the case that the product almost blocks the catalyst ($K_{C_mH_n} p^0_{C_mH_{n+2}} = 10$). Here the denominator would increase by one order of magnitude at full conversion. With increasing inhibition the curves are shifted upwards because the reaction rate is lowered.

Curve (F) refers to the same parameters as curve (E) but in the ideal membrane reactor with complete removal of hydrogen. Due to the strong inhibition the reaction rate is lower than for curve (A), but the reaction can be carried out until completion. The influence of the preferred adsorption of the product on the effectiveness of the membrane reactor is shown more directly in Fig. 26, which gives the integrals of the curves belonging to the cases (A/B) and (F/E) of Fig. 25 as a function of the conversion. For clarity of the graphic representation a less diluted hydrocarbon feed was assumed ($p^0_{C_mH_{n+2}} = 50\,\text{kPa}$) resulting in a reduced equilibrium conversion of 57.5% at unchanged value of K_p (30 kPa).

Point (1) denotes a suitable operating point of the conventional packed-bed reactor close to the equilibrium conversion. It refers to the case without inhibition by adsorption. The point labelled (2) marks the same reference conversion but for the case with strong adsorption of the target product, i.e. $K_{C_mH_n} p^0_{C_mH_{n+2}} = 10$, which would require a 4.5 times higher catalyst volume. The calculation for an ideal membrane reactor having the same catalyst volume gives a conversion of $X_2^* = 78\%$ at point (2*). Without inhibition by

adsorption of the product the conversion of the membrane reactor is found at point (1*) and would be $X_2^* = 87\%$ as compared to 56% for the conventional packed-bed. Comparing the values of X_1^* and X_2^* underlines that a preferred adsorption of the target product can decrease the expected benefit of a membrane reactor.

2.4.5. Current status of membrane reactor experiments for hydrocarbon dehydrogenation

There is no doubt about the usefulness of qualitative estimations and detailed kinetic simulations in trying to assess the potential of palladium-based membrane reactors, but at the end experiments have to confirm the theoretical predictions and so an evaluation of the available experimental results is useful to complete this report. Palladium-based membranes were tested in the past in numerous reactions with removal or supply of hydrogen to packed-bed catalysts (cf. [19,20]). We do not attempt to review the whole field but restrict ourselves to hydrocarbon dehydrogenation, and here to representative applications where the literature contains a substantial body of experimental data.

2.4.5.1. Dehydrogenation of cyclohexane to benzene. One of the early applications of palladium membrane reactors was the dehydrogenation of cyclohexane to benzene [84–87]. Itoh [85] used a palladium tube with 200 μm wall thickness, 140 mm length and 17 mm diameter. The tube was uniformly packed with cylindrical pellets of a noble metal catalyst (3.3 mm × 3.6 mm). The reaction conditions were 200°C and 100 kPa, and the cyclohexane was diluted by argon. Argon was utilised also as a sweep gas. It was shown that the conversion of cyclohexane in the membrane reactor can be increased to nearly 100% at sufficiently large residence times and by using enough sweep gas. However, the space velocity was very low in these experiments (GHSV = 0.7–4.2 h^{-1}) and so was the hydrogen generation rate per unit volume (R_{H_2} = 0.03–0.12 mol/m^3 s). In view of the low reaction rate the low hydrogen flux through the 200 μm thick palladium tube wall was still sufficient not to limit the performance of the membrane reactor. The mole fraction of cyclohexane in the feed was 19.7% and an equilibrium conversion of 18.7% was detected in a conventional packed-bed reactor. From these values the hydrogen partial pressure at the equilibrium is estimated to 10 kPa and hence, according to the permeation kinetics given, the maximum hydrogen flux through the membrane is 1.87×10^{-3} mol/m^2 s. This finally gives a minimum required membrane area of 57 m^{-1} corresponding to a tube diameter of 70 mm. The actual tube diameter was 17 mm, which confirms that the membrane is not expected to limit the performance.

In later studies Itoh and Wu showed experimentally for the same system under similar reaction conditions and using a palladium–silver tubular membrane (length 191 mm, diameter 10.4 mm and wall thickness 0.2 μm) that the permeated hydrogen can be removed efficiently by passing an oxygen-containing sweep gas through the permeate compartment, and that the heat produced by oxidation of the hydrogen leads to an increase of the packed-bed temperature in a quasi-adiabatic operation [86,87]. No particular excess of the oxygen-containing sweep gas flow over the cyclohexane flow is required except that the amount of oxygen supplied must be high enough to convert all the permeated hydrogen.

These results nicely demonstrate the benefits of hydrogen removal in a palladium membrane reactor. However, the cyclohexane system must be seen primarily as a model reaction without immediate significance for an industrial application.

2.4.5.2. Dehydrogenation of methylcyclohexane to toluene. A similar reaction, but with some technological background, is the dehydrogenation of methylcyclohexane to toluene, which was investigated by Ali et al. [33] in the context of the usage of hydrogen as secondary energy carrier. The concept is as follows: toluene, acting as a hydrogen carrier, is hydrogenated to methylcyclohexane with hydrogen produced from hydroelectric power to store the energy in an organic liquid. Upon demand methylcyclohexane is catalytically dehydrogenated and the released hydrogen can be used for stationary or mobile electricity generation.

The membrane reactor used in the experimental studies was a 250 mm long stainless steel tube with an inner diameter of 15.8 mm. A palladium–silver tube of 3.1 mm diameter and 200 μm wall thickness, closed at one end, was placed in the centre line of this reactor. The reactor was charged with a commercial noble metal catalyst of about 1 mm particle size diluted with

spherical glass beads (bulk catalyst volume 4.15 cm^3). The reaction was studied in the temperature range of 300–400°C at reaction pressures of 0.5–2 MPa and liquid hourly space velocities of 2–12 h^{-1}. The permeate pressure was slightly above the atmospheric level because no sweep gas was employed.

It could be shown that in the membrane reactor conversions significantly above the equilibrium value can be achieved, despite that the hydrogen permeation rate was reduced by about 14% in presence of the organic products. For example, at 1.5 MPa and 340°C the conversion of methylcyclohexane was 48% at LHSV = 10.2 h^{-1}, 59.5% at LHSV = 6.5 h^{-1}, and 80% at LHSV = 3.6 h^{-1} compared to the equilibrium value of 42%. The lower efficiency of the membrane reactor at high space velocities can be traced back to the limiting hydrogen permeance. This becomes evident if the hydrogen generation rate is compared to the hydrogen permeation rate. Upon increasing the space velocity from 3.6 to 10.2 h^{-1} the hydrogen generation rate per unit volume was raised from 1.85 mol/m^3 s almost linearly to 3.2 mol/m^3 s, whereas the permeation rate increased only initially a little from 0.0312 to 0.0347 mol/m^2 s. The membrane area per unit volume required for a match of the hydrogen generation and permeation rates is 59.3 m^{-1} for LHSV = 3.6 h^{-1} and 92.2 m^{-1} for LHSV = 10.2 h^{-1}. In the membrane reactor 22.9 cm^2 of membrane area were available for a packed-bed volume of 41.5 cm^3, which gives a volume-based membrane area of 55.2 m^{-1}. This shows that for low space velocities, i.e. below LHSV = 3 h^{-1}, the available membrane area is more or less sufficient, whereas for higher space velocities the produced hydrogen cannot be removed fast enough. A better performance of the membrane reactor at higher space velocity can be expected if a membrane with reduced thickness of the palladium–silver layer is available. An alternative is to increase the membrane area inside the reactor or to reduce the amount of catalyst per unit volume (higher dilution of the packed-bed).

Even though the performance in this system obviously is limited by the membrane, the results show that a palladium membrane reactor can give higher conversions than the equilibrium values also at industrially feasible space velocities, provided that the reaction rate is high enough. The membrane and the catalyst were stable for more than 300 h on stream with intermittent shutdown of the methylcyclohexane feed overnight (i.e. replacement by hydrogen) and with temperature cycling, and it could be shown that the membrane and the catalyst can be liberated from contaminants by oxidation in air.

However, one must be aware of the fact that the catalyst has been diluted 10 times with glass beads so that the space time yield of the reactor is still low. In a real application working without dilution in the same range of the space velocity would require much better membranes or a much higher membrane area per unit volume.

Ali and Baiker [88] reported additional results on this system a few years later, where they used an undiluted catalyst bed (1.6 mm particle size and 43.1 cm^3 bed volume) and a palladium–silver membrane of reduced wall thickness (100 μm). The length (230/239 mm) and the diameter (3.1 mm) of the membrane were unchanged. The reactor temperature and pressure were similar as in the previous study, i.e. 320–400°C and 1.5 MPa (0.1 MPa permeate pressure), whereas the space velocity was reduced to 0.5–2.6 h^{-1}. Also under these conditions the membrane reactor gave conversions above the equilibrium, e.g. 90% versus 73.3% at 370°C and LHSV = 1 h^{-1}. The conversion increase was more pronounced at low temperatures where the equilibrium restriction is more severe. However, the conversion declined more strongly with increasing space velocity in the membrane reactor than in the conventional packed-bed, which still indicates a limitation by the permeance. A quantitative analysis showed that the membrane was able to remove most of the produced hydrogen only at space velocities below LHSV = 1 h^{-1}. At higher space velocities the reactor performance became more and more controlled by the permeation rate and hence the conversion increase was suppressed. Low space velocities are unattractive for industrial operation because they are connected to low space time yields. An optimum space velocity of 1.65 h^{-1} at 370°C was reported as a compromise with regard to high conversion and high reaction rate. Under these conditions the membrane reactor reached 78% conversion compared to the equilibrium conversion of 73.3%. The reference conversion in a conventional reactor was 65%. Putting the hydrogen generation rate (8.4 mol/m^3 s) in relation to the permeation rate (0.103 mol/m^2 s) shows that a membrane area per unit volume of 81 m^{-1} would

have been required for a match of both. The membrane reactor used had only 22.9 cm^2 membrane area for a total packed-bed volume of 41.3 cm^3, which is equivalent to a value of 55.4 m^{-1}. This confirms the limitation by the permeation rate. The hydrogen flux through the membrane was about three times higher than in the previous study, but due to the undiluted catalyst bed the hydrogen generation rate per unit volume was increased likewise, i.e. by a factor of 2.6–4.5 depending on the point of reference (LHSV = 3.6 or 10.2 h^{-1}). A second limitation of the performance of the membrane reactor was by the heat input. The temperature of the undiluted catalyst bed dropped significantly at high reaction rates (high space velocity) as a matter of the strong endothermicity of the reaction ($\Delta H_R > 200$ kJ/mol).

The final conclusions from the work on methylcyclohexane dehydrogenation are that the effectiveness of the membrane reactor could be further increased by the use of better membranes, i.e. with reduced thickness of the palladium layer, in order to overcome the limitation by the permeation rate. Obviously an excellent catalyst is available which does not suffer from the adsorption of the product toluene and the associated decrease of the reaction rate at high conversions (cf. [89] and the discussion in the previous section). The results have been obtained under industrially relevant space velocities and with realistic feed concentrations and operating pressures. Hence, they seem to prove the technical feasibility of a palladium-based membrane reactor for this reaction. Long-term studies will have to demonstrate the performance over a realistic period of time, and the detected heat transfer limitation may require a more sophisticated reactor module design, but the main problem still is the high palladium thickness of the commercial palladium–silver membranes, which are not economically viable due to the high price of the palladium.

2.4.5.3. Dehydrogenation of alkanes to olefins. A variety of *n*- and isoalkane dehydrogenations have been studied experimentally in palladium-based membrane reactors. Among those reactions propane dehydrogenation has probably received the most interest over the last years. Other feedstocks have been, for example, ethane, *n*-butane, isobutane or isopentane. Alkane dehydrogenations are industrially important reactions since the olefins produced represent basic petrochemical building blocks, e.g. for the manufacture of plastics. These reactions all need high temperatures to proceed at reasonable rates and to shift the conversion to levels of practical significance. Another feature they have in common is the formation of carbon deposits which must be prevented or at least diminished to an acceptable level.

Sheintuch and Dessau [90] studied the dehydrogenation of isobutane and propane in packed-bed membrane reactors equipped with commercial tubular palladium–silver (25% Ag) or palladium–ruthenium membranes (2% Ru), respectively. The latter had a length of 305 mm, an outer diameter of 6.35 mm and a wall thickness of 254 μm, whereas the former was 203 mm long and 3.2 mm thick and had a wall thickness of 76 μm. Both membranes were inserted in stainless steel shells and sealed at the ends by fitting T junctions. The membrane tubes were packed with 0.5–1 g of a fine-grained supported platinum catalyst (0.52 wt.% Pt) diluted with pyrex particles of similar grain size. Nitrogen was supplied as a sweep gas on the shell side to establish the driving force for the hydrogen permeation.

The performance of the membrane reactor turned out to be strongly dependent on the flow rates of the reactants and the sweep gas. During isobutane dehydrogenation at 500°C and atmospheric pressure, high reactant flow rates together with high sweep gas flow rates in the palladium–ruthenium membrane reactor caused only a moderate increase of the conversion over the equilibrium value of 32.4%; the catalyst activity was more or less stable. Decreasing the reactant flow rate and increasing the sweep gas flow rate led to a rapid deactivation which could be traced back to a complete removal of hydrogen from the packed-bed. Under optimised conditions, i.e. at a low reactant flow rate of 1 ml/min and a moderate sweep gas flow rate of 230 ml/min a maximum conversion of 81.2% was reached (total yield of butenes: 75.9%). Under these conditions a small amount of hydrogen (below 1–2%) remained on the tube side which is believed to accelerate the reaction rate and to stabilise the catalyst against carbon deposition. The hydrogen level was found to be critical for the performance of the catalyst: too high hydrogen concentrations inhibit the reaction rate, whereas too low hydrogen concentrations lead to an accelerated deactivation.

This behaviour was even more pronounced during the dehydrogenation of propane, most likely because of the higher reaction temperature of 550–570°C. Compared to the equilibrium propylene yield of 32% at 550°C and atmospheric pressure, the propylene yield in the palladium–ruthenium membrane reactor operated at a reactant flow rate of 1 ml/min reached 70%. The yield declined more rapidly with time in the palladium–silver membrane reactor than in the palladium–ruthenium membrane reactor, which was attributed to the faster hydrogen removal (lower wall thickness and higher membrane area per unit volume) accelerating the deactivation rate of the membrane and the catalyst. Moreover, the initial propylene yield was also lower in the palladium–silver membrane reactor, which was explained by an inhibition of the reaction rate at infinitely small hydrogen concentrations. At 550°C and atmospheric pressure the palladium–silver membrane reactor gave only 47.5% propylene yield as opposed to 70% with the palladium–ruthenium membrane under similar conditions. The authors showed that under optimised conditions, i.e. at low reactant flow rates and moderate sweep gas flow rates, when a sufficient amount of hydrogen is still present on the packed-bed side, the membrane reactor can maintain a rather constant propylene yield over a period of 50–100 h. Under more severe conditions the activity of the catalyst and the hydrogen flux through the membrane both decline more quickly as a matter of the deactivation by carbon deposition. Concerning the membrane it was demonstrated that the deposits on the surface can be removed and the original hydrogen flux can be restored by a treatment in a hydrogen-rich atmosphere at temperatures around 500°C. Unfortunately, the catalyst cannot be fully regenerated by this treatment.

Both for isobutane and propane dehydrogenation it was demonstrated that working at elevated pressure (222 and 788 kPa) suppresses the equilibrium conversion but at the same time enhances the hydrogen flux through the membrane. The consequence is that the equilibrium shift is more pronounced at higher pressure even though the absolute conversion of the membrane reactor is still a little bit lower than at atmospheric pressure. However, high pressure on the packed-bed side can be interesting because this allows to work without sweep gas and provides pure hydrogen. Simulations were carried out based on the measured kinetics of the reaction and the permeation to identify an optimum set of operating parameters for the membrane reactor. The results confirmed that working at elevated pressure may lead to similar propylene yields than at atmospheric pressure but not to an increase of the propylene yield. Moreover, it became clear that as long as thick-walled commercial membranes are used a significant increase of the propylene yield can be expected only at low reactant flow rates, i.e. space velocities in the range of LHSV = 0.1–0.15 h^{-1}, which are about 5–10 times below those used in industrial units. High yields at higher space velocities would require membranes with much better hydrogen fluxes, e.g. thin-walled palladium composite membranes.

Collins et al. [32] performed studies on propane dehydrogenation in different membrane reactors equipped with thin-film microporous silica-based membranes or with palladium composite membranes at industrially relevant space velocities of LHSV = 2–12 h^{-1} and temperatures in the range of 500–575°C. The membranes were developmental membranes, i.e. the palladium composite membranes had a higher hydrogen permeance than commercial palladium alloy tubes and the silica-based membranes showed higher selectivities than commercial ceramic membranes.

The palladium membranes were made by electroless plating. Commercial tubular alumina microfiltration membranes of 10 mm o.d. and 7 mm i.d. served as supports. The palladium coating was placed on the inner side and had a thickness of about 12 μm. The catalyst was a platinum-loaded aluminosilicate molecular sieve (Amoco Corp.), which was packed inside the membrane. The tube-side pressure during the membrane reactor experiments was around 100 kPa, whereas the shell side pressure was 90.5 kPa. The reactor feed consisted either of pure propane or a mixture of 80% propane and 20% hydrogen. Nitrogen was used as a sweep gas, and the ratio of the inlet sweep gas flow to the propane feed flow was varied between 2 and 8.

The hydrogen permeance of the palladium composite membrane was measured with pure gases at the beginning. Then a membrane reactor experiment was carried out with a mixed propane/hydrogen feed (80/20) at a space velocity of LHSV = 2.26 h^{-1} and a fixed sweep gas to feed ratio of 2. The temperature was initially set to 500°C and afterwards increased in steps of 25 K up to 575°C with 3 h holding time in

each case. During the experiment the hydrogen permeance was determined in order to check the membrane performance. It was surprisingly found that the permeance decreased at higher temperatures. Moreover, the membrane was deactivated when exposed to reaction conditions. In the membrane reactor the palladium membrane showed a lower hydrogen permeance than a silica-based membrane even though its initial hydrogen permeance was higher. It was also noticed that after the temperature had been raised to 525°C the leakage rates of propane and propylene increased significantly. SEM micrographs later showed small holes in the surface of the palladium layer which proved that the membrane was not stable under these conditions. At 500°C when the palladium layer was still intact the membrane reactor gave a propylene yield of about 16% compared to 12% obtained in a conventional packed-bed reactor under the same conditions (the calculated equilibrium conversion for a feed with 20% hydrogen and 80% propane is 10.5%). At higher temperatures the yield increase over the conventional reactor gradually diminished, which was explained by the reduced hydrogen permeance. At 575°C no difference in the propylene yield was found between the palladium membrane reactor and the conventional reactor. The selectivity to propylene was generally above 97%. No marked differences of the selectivity were found between the membrane reactors and the conventional reactor. In additional experiments the authors noticed a formation of carbon deposits on the palladium surface during contact with propane (no hydrogen added) at high temperature, and in particular, when propylene was present. They also found in permeation experiments that an addition of propylene reduces the hydrogen flux significantly. These observations led them to a preliminary explanation for the failure of the membrane, that carbon deposition from propylene first causes a deactivation of the palladium surface and then the incorporation of carbon into the palladium film, or rather the stress associated with this, leads to the formation of pinholes.

The authors also studied the deactivation behaviour of the catalyst in the membrane reactor (silica-based membranes). The deactivation in the membrane reactor proved to be faster than in a conventional reactor if most of the produced hydrogen was removed by the membrane, e.g. over a period of less than 9 h at 550°C and LHSV $= 3\,h^{-1}$ the propylene yield decreased from 39.6 to 31.5%. However, when operated at higher space velocities and with a lower sweep gas to feed ratio the deactivation rate was reduced to the same level as in the conventional reactor, if not below. Hence, it seems possible by proper choice of the process parameters that the membrane reactor can maintain a higher propylene yield than a conventional reactor over the whole dehydrogenation cycle.

Weyten et al. also studied propane dehydrogenation in membrane reactors equipped with silica composite membranes [91] and with a palladium–silver composite membrane, respectively [74]. The palladium–silver membrane was obtained from Johnson Matthey and is said to be commercially available. It was a tubular membrane of 25 mm o.d., cut to 200 mm length, which had a 7.5 μm thick palladium–silver film on the outer surface of an asymmetric alumina support with 2 mm wall thickness. The palladium–silver film was prepared by electroless plating, and the effective membrane area was $140\,cm^2$. A conventional chromia-alumina catalyst with a grain size of 0.2–0.5 mm was packed inside the membrane tube (total amount 21 g). Experiments were performed with undiluted propane at 500°C and atmospheric pressure on the tube and shell side. An inert sweep gas (nitrogen) served to establish the driving force for the hydrogen permeation.

The membrane reactor reached propane conversions above the equilibrium level of about 18% only if the space velocity was lower than WHSV $= 0.8\,h^{-1}$. The selectivity to propylene was generally between 85 and 95%. It was always higher than in a conventional packed-bed reactor under the same operating conditions. This is explained by a reduced extent of cracking reactions producing methane and C_2-hydrocarbons if hydrogen is removed. At extremely low space velocities in the range of WHSV $= 0.05$–$0.1\,h^{-1}$ propane conversions of 60–80% were detected, but under these conditions the growing influence of the cracking reactions caused a reduced propylene selectivity. If the space velocity was increased above WHSV $= 0.8\,h^{-1}$ the membrane reactor gave only the equilibrium conversion, indicating that the performance was controlled by the thermodynamics, i.e. the permeation rate of hydrogen was too slow compared to the rate of hydrogen generation.

It should be mentioned that the propane conversions reported were calculated from the mole fractions of

propane in the feed and the retentate stream, i.e. $X_i = 1 - x_i/x_i^0$, which is true only if the number of moles does not change during the reaction. In a conventional reactor without removal of hydrogen the total number of moles increases linearly with conversion. Hence, for a pure propane feed a conversion of $X_i = 0.5$ determined from the decrease of the mole fraction is equivalent to a true conversion between 0.25 (no hydrogen removal) and 0.5 (removal of the entire hydrogen).

The deactivation of the catalyst was not studied in detail. The authors just noted that at 500°C the catalyst was stable for at least 7 h before its activity gradually decreased to 50% of the initial value after 30 h, and that it can be easily regenerated by burning off the coke at 500°C overnight in a mixture of 4% oxygen in nitrogen. The membrane apparently was stable under the operating conditions tested, i.e. neither a decrease of the hydrogen permeance nor a reduction of the separation factor was reported.

Yildirim et al. [31] compared the performance of different membrane reactors for dehydrogenation of propane, i.e. dense palladium–silver composite membranes and asymmetric porous alumina membranes with incorporated palladium clusters. The porous alumina membranes were modified by silica deposition and subsequent impregnation with palladium chloride. After washing and drying the membranes were treated under hydrogen flow at 400°C in order to reduce the palladium chloride to metallic palladium. The dense palladium–silver membrane was prepared by magnetron sputtering on a tubular porous Vycor glass membrane (10 mm o.d., 200 mm length, 1.1 mm wall thickness and 4 nm pore size) and had a palladium thickness above 4 μm. The tubes were packed with 2.55 g of either 0.5 wt.% Pt/Al_2O_3 or 0.5 wt.% Pd/Al_2O_3 cylindrical catalyst pellets (3.4 mm × 3.6 mm). In case of the palladium–silver membrane 18.5 cm^2 membrane area were available per gram of catalyst. With this membrane experiments were carried out only at a temperature of 400°C. Higher temperatures were avoided to prevent carbon deposition. Different sweep gases were applied, i.e. nitrogen, carbon monoxide and air. The space velocity, as calculated from the specified propane concentration at the inlet, the flow rate and the given catalyst amount, was in the range of WHSV = 0.7 h^{-1}. The transmembrane pressure difference during the experiments is not given, but it is stated that without a sweep gas only a moderate increase of the conversion was detected. With nitrogen as a sweep gas the membrane reactor gave a propane conversion of 17.5%. The conversion was further increased to 38% when a mixture of carbon monoxide and nitrogen (11% CO) was used, and with air as reactive sweep gas a propane conversion of 51% was detected. Although measurements of the hydrogen concentration in the effluent from the packed-bed side are not given, these results demonstrate that the palladium surface can be utilised to react the permeated hydrogen with a sweep gas so that a high driving force for the permeation is established.

The long-term behaviour of the membrane under reaction conditions was not studied in detail, but permeation experiments with temperature cycling proved that the membrane was stable.

Quicker [61] also studied propane dehydrogenation in a palladium composite membrane reactor. The membranes were prepared by electroless plating on asymmetric porous ceramic tubes and by a combined electroless/electroplating on asymmetric porous sintered stainless steel tubes. The stainless steel tubes were alternatively coated by thermal spraying of palladium powder (high-velocity oxy-fuel flame spraying (HVOF)). Both types of supports had a similar geometry, i.e. 10 mm o.d., 110 mm length and 1.5–2 mm wall thickness. The palladium coating on the alumina support was placed on the tube side and was 2–3 μm thick, whereas the palladium layer on the sintered stainless steel support was placed on the shell side and had a thickness of roughly 8 μm (plating) and 60–70 μm (HVOF), respectively. The membrane tube and a surrounding dense tube (alumina or stainless steel) of 21 mm i.d. were inserted into a stainless steel jacket and screwed up with the help of two stainless steel flanges connected to the gas lines (cf. Fig. 4). Graphite gaskets were used for sealing the tubes to the flanges. An amount of 17 gramme of a chromia-alumina catalyst (Linde AG, grain size 0.8–1.0 mm) was placed in the annular space between the membrane tube and the dense tube. Dehydrogenation experiments were carried out at 560°C and pressures of 130 kPa on the packed-bed side and 110 kPa on the permeate side in each case over a period of several hours. Pure propane was fed at a space velocity of WHSV = 0.7 h^{-1}, while nitrogen was employed as sweep gas. The ratio of the sweep gas linear

flow velocity to the propane linear flow velocity (i.e. the *normalised* sweep gas flow) ranged between 17 and 27.

The calculated equilibrium conversion of propane at 130 kPa and 560°C is 30.2%. In the conventional packed-bed a conversion of 29.2% was detected. The palladium–alumina membrane reactor reached 34.7%. With the plated palladium–stainless steel membrane 46.5% were achieved, and with the palladium–stainless steel membrane prepared by HVOF the conversion was 38.5%. Comparing the propylene yields is more instructive: 22.4% were reached in the conventional packed-bed, 27.8% with the palladium–alumina membrane, 26.7% with the plated palladium–stainless steel membrane and 25% with the palladium–stainless steel membrane prepared by HVOF. Two things are apparent from this: first the selectivity to propylene was lower than in the commercial process (>90–95%) which is due to the lower space velocity used. Second the selectivity to propylene was much lower with the stainless steel-based membranes than with the palladium–alumina membrane. The amount of gaseous side products (mainly C_1 and C_2 hydrocarbons) was similar in all experiments so that the reason was an enhanced carbon deposition on the membrane, which was witnessed also by a decline of the hydrogen permeance with time. Similar observations were described by Sheintuch and Dessau [90]. The carbon deposition rate found with the palladium–stainless steel membranes was five times higher than with the palladium–alumina membrane. The latter was similar to the carbon deposition rate in the conventional packed-bed. The distribution of the produced hydrogen between the retentate and permeate side reveals that the palladium–stainless steel membranes were able to recover a larger fraction of hydrogen (plated: 68% and HVOF: 59%) compared to the palladium–alumina membrane (38%). The lower hydrogen concentration in the retentate can be one reason for the increased carbon deposition rate, but it is more likely that the different location of the palladium layer is responsible. The palladium layer was adjacent to the catalyst bed in case of the palladium–alumina membrane and near the catalyst in case of the palladium–stainless steel membranes. The regeneration of the composite membranes by oxidation was not studied.

The experimental results obtained on the dehydrogenation of propane in palladium-based membrane reactors may be altogether summarised as follows.

At low space velocities conversions well above the equilibrium level have been obtained both with thick-walled palladium alloy membranes and with palladium or palladium–silver thin-films supported on porous glass or porous ceramic tubes. Thick-walled palladium alloy membranes do not allow sufficient hydrogen fluxes to achieve a significant conversion increase at industrially used space velocities, e.g. WHSV $= 1.2$–$2.0\,h^{-1}$. With thin-film palladium alloy membranes prepared by electroless plating promising results have been obtained, but the permeance still limited the performance of the membrane reactor at space velocities above WHSV $= 0.8\,h^{-1}$. This indicates that higher membrane areas or thin-film membranes with better hydrogen permeances are required. It is also possible that the permeance in the membrane reactor is reduced to some extent by adsorption of reactants or poisoning of the membrane surface (carbon deposition).

Thick-walled palladium alloy membranes have shown reasonable stability against high temperature and the reactant atmospheres, in some studies with thin palladium or palladium alloy films deposited by electroless plating stability problems have been encountered at temperatures above 400–500°C. Coke deposition initiated by propylene is suspected to cause pinholes in these layers due to incorporation of carbon. However, other studies using similar membranes gave no indications of membrane failure, though carried out at temperatures below 500°C and for short-term only. Generally, little information is available about the long-term performance of thin-film palladium-based membranes used in membrane reactors for alkane dehydrogenation. Moreover, the service life of the catalysts at hydrogen depleted conditions is not sufficiently clear.

All three options to generate the necessary driving force for hydrogen permeation, i.e. inert sweep gas, transmembrane pressure difference, and reactive sweep gas have been proved in the lab-scale in principle. However, in most studies inert sweep gas or a transmembrane pressure difference are applied. The use of a reactive sweep gas, which could provide the heat for the endothermic reaction, is less well demonstrated, in particular because in all cases small tubes

have been used where the heat management is not critical.

2.4.5.4. Dehydrogenation of ethylbenzene to styrene. Another reaction of great industrial importance is the dehydrogenation of ethylbenzene to styrene which has served as a model reaction for the use of equilibrium shift membrane reactors in many simulation studies. However, experimental work on membrane reactors for ethylbenzene dehydrogenation in the past focused mainly on commercial porous membranes with Knudsen-type separation behaviour. Only recently experiments using palladium composite membranes for dehydrogenation of ethylbenzene were reported. Quicker et al. [60,61] used palladium–alumina membranes prepared by electroless plating (2–3 μm layer thickness) in the same reactor as reported in the previous section. The reactor was filled with 20 g of a commercial iron oxide catalyst (Süd-Chemie AG, grain size 0.8–1.0 mm) and was operated at 580°C with a space velocity of WHSV = $1\,h^{-1}$ and a steam to ethylbenzene ratio of S/O = 2:1 kg/kg. The retentate pressure was set to 110 kPa while the permeate pressure was kept at 100 kPa. Nitrogen was employed as a sweep gas. The normalised sweep gas flow ranged from 0 to 105. It was demonstrated that the conversion of ethylbenzene was increased from 39 to 45% at the maximum sweep gas flow while the selectivity to styrene was constant at 93–93.5%. The calculated equilibrium conversion at these conditions is 71.7%. The analysis of the hydrogen split between the retentate and the permeate at the reactor exit showed that even at the highest sweep gas flow only about 1/4 of the produced hydrogen was in fact transported through the membrane. This suggests a limitation by the permeance. However, at present no concluding statement can be made because data are not yet available from experiments at different space velocities and in the above experiments the equilibrium conversion was not reached.

She et al. [92] used a palladium composite stainless steel membrane to enhance the dehydrogenation of ethylbenzene by removal of hydrogen in a membrane reactor. The membrane had a 20 μm thick palladium layer and an effective membrane area of 75 cm^2. Argon was used as sweep gas at ambient pressure. At 550°C and 120 kPa with a steam to oil ratio of 6.8 the conventional reactor reached a conversion of 35%, whereas the membrane reactor achieved 45%. The space velocity and the amount of hydrogen removed is not given in [92], but the calculation of the equilibrium conversion for the experimental conditions applied (51.7%) indicates a similar situation as in the experiments performed by Quicker [61].

Hence, it must be stated that the experimental results obtained so far on ethylbenzene dehydrogenation in palladium composite membrane reactors are still very limited. No supra-equilibrium conversions have been reported. The main question once more in this application is the stability of the membranes against the reactant atmosphere (steam, styrene) at high temperatures. Moreover, it has to be demonstrated at which space velocities the equilibrium conversion can be surpassed.

This leads to the final conclusion that the main problem for the experimental investigations still is the non-availability of membranes that can withstand the required temperatures and gas atmospheres. Thick-walled palladium alloy tubes have shown good performance at low space velocities and also a reasonable stability mainly in model dehydrogenation reactions, but for real applications they have no perspective due to the high palladium price and the low permeance. Despite obvious progress in the preparation and characterisation of thin-film palladium and palladium alloy membranes the experimental work applying these membranes to industrially relevant dehydrogenation reactions is still in its infancy. The few available results from experiments in membrane reactors under realistic process conditions indicate that these membranes are susceptible to pinhole formation at high temperatures and to failure by carbon deposition, in particular under hydrogen depleted conditions. The membranes are not commercially available on a regular basis, and with very few exceptions (e.g. [36]), all the experimental investigations have been carried out in the lab-scale. It is not clear how membranes with larger areas can be produced economically, and at the present price of palladium already a 1 μm thick palladium layer would cost about 400–450 €/m^2 (without support). Because 1 μm thickness is probably not sufficient for a stable and defect-free membrane this means that such a technology-provided it can be successfully demonstrated-is interesting only for valuable products or when a compact design (‘intensified process’) is of foremost importance.

3. Membrane reactors based on porous catalytic membranes with dispersed palladium

Porous membranes with built-in catalytic components are catalytic membranes in the true sense of the word. They can be employed in a reactor in various ways, which may be classified into the following three categories:

1. Forced flow of (pre-mixed) reactants through the membrane.
2. Co-current or counter-current flow of two reactant streams on opposite sides of the membrane with permeation of all species across the membrane (non-permselective).
3. Co-current or counter-current flow of two reactant streams or a feed stream and a sweep stream on opposite sides of the membrane with selective permeation of particular species across the membrane.

The most simple is configuration (1) which is not a membrane reactor in the strict sense of the IUPAC-definition because it has no separation by the membrane. The contact time per pass in such a design is usually short. Hence, the reaction has to be very fast or the reactants have to be passed through the membrane many times, e.g. by applying a reactant recycle.

Configuration (2) stands for the CNMR-concept, i.e. the membrane provides a defined interface for the reaction of the two feed streams. Here, the reaction has to be very fast too because a breakthrough of the respective species to the opposite side is unwanted.

Configuration (3) certainly is the most relevant one with regard to catalytic membrane reactors. It requires a permselective membrane. However, in a gas–liquid reaction permselective transport through the membrane can occur also when the gas–liquid interface is arranged inside the porous membrane. Such a concept may be called *catalytic diffuser* and is of general applicability in fast solid-catalysed gas–liquid reactions. Liquid-phase hydrogenation on palladium catalysts represents an industrially important class of reactions that falls into this category.

3.1. Working principle of a catalytic diffuser

In the catalytic diffuser a gas stream and a liquid stream are supplied on opposite sides of a porous membrane with good wettability. The membrane has an asymmetric structure with the coarse support on the gas side and the fine layer on the liquid side. Due to the capillary forces the liquid is sucked into the pores of the fine layer. The liquid is stopped at the point where the capillary pressure, that depends on the pore size and the pore geometry, is equalled by the pressure difference between the gas side and the liquid side (cf. Fig. 27). The catalyst is placed on the pore walls of the fine layer, e.g. in the form of highly dispersed clusters, whereas the support has no catalyst inside. A uniform pore size of the fine layer is

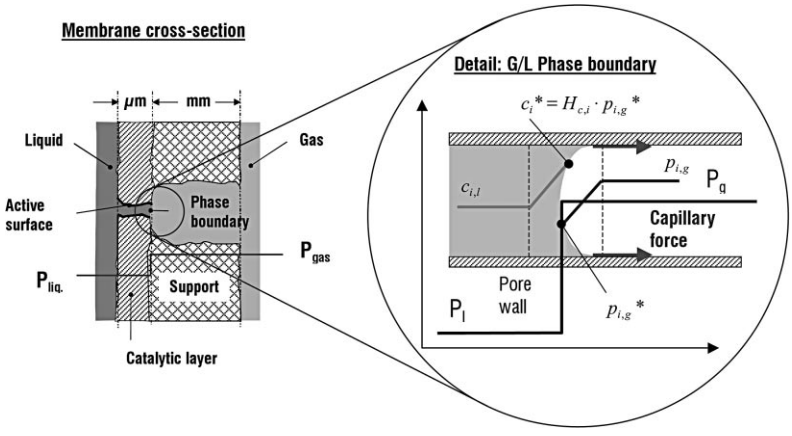

Fig. 27. Working principle and arrangement of the active phase in a catalytic diffuser. At the gas–liquid phase boundary in the pores, the capillary pressure is equal to the pressure difference between the gas and the liquid.

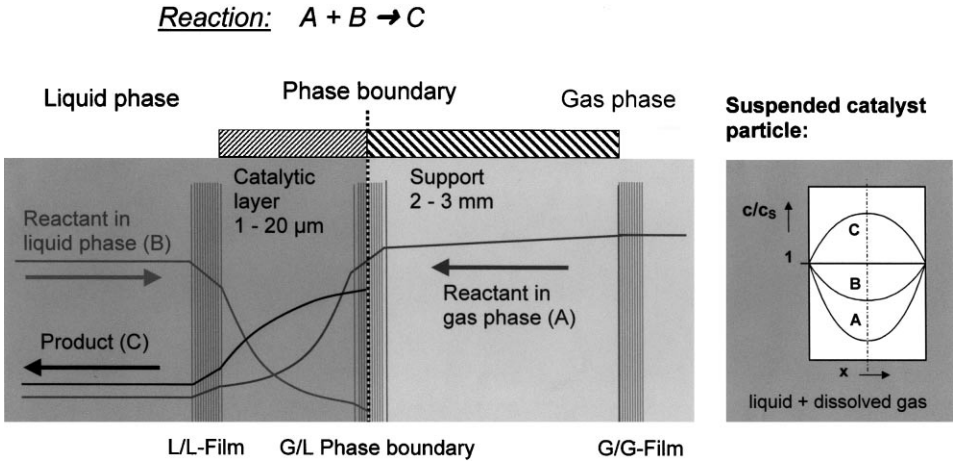

Fig. 28. General shape of the concentration profiles in the reaction zone of the catalytic diffuser for a hypothetical reaction A + B → C. Comparison with the concentration profiles in a suspended catalyst particle.

beneficial because this allows a good control of the location of the phase boundary. The total effective area of the gas–liquid interface is of the order of the membrane surface area.

The gas diffuses through the coarse support and is taken up by the liquid at the gas–liquid interface. The dissolved gas then diffuses through the liquid-filled pores of the fine layer towards the liquid side. The reaction between dissolved gas and the liquid or dissolved species in the liquid occurs at the active clusters on the pore walls. The reaction products diffuse out towards the liquid side following the pressure gradient. Typical concentration profiles of the gaseous and liquid reactants inside the catalytic layer are shown in Fig. 28 together with concentrations profiles that would be obtained in a conventional suspended catalyst particle. The following advantages of the catalytic diffuser compared to a suspended catalyst may be summarised:

- The catalyst is immobilised in the membrane, i.e. no fine catalyst particles have to be used. The catalytic layer can be made thin enough so that pore diffusion limitation is avoided.
- The two reactants can be supplied from opposite sides to the catalytic region, that is the supply rates can be controlled independently of each other. In particular the gas pressure can be varied between the bubble point pressure of the support and that of the fine layer. This allows to adjust the gas supply rate to the (varying) needs of the reaction.
- Auxiliary substances can be supplied directly to the catalytic region without passing through the bulk liquid (avoiding possible mass transfer limitations).
- No saturator is required before the reactor to dissolve the gas in the liquid.
- Even if the solubility of the gas in the liquid is poor high pressure is not required in the reactor because the gas is supplied directly to the region where it is consumed.

3.2. Application of catalytic diffusers to the hydrogenation of nitrate in water

The hydrogenation of nitrate in water on bimetallic palladium-based catalysts has been first proposed more than a decade ago by Vorlop and co-workers as an alternative method for nitrate removal from groundwater and surface water [93–96]. Based on this work a process called ‘catalytic nitrate reduction’ was developed by Solvay Umweltchemie GmbH, Hannover (Germany) [97]. A comprehensive review of the process development from the beginning until today has been provided recently by Lecloux [98]. He describes the catalyst development at the lab scale including kinetics and molecular modelling equally like chemical engineering aspects such as mass transfer and reactor design until to practical difficulties that were

encountered in field tests. Details on the preparation and the performance of bimetallic catalysts used for nitrate reduction in water are reported in another contribution to the present volume by Prüße, who gives also an introduction to the general background of nitrate reduction in water. The most important features of the reaction are briefly summarised below.

Nitrate ions are reduced by hydrogen via a number of successive reactions until to the target product nitrogen. The reaction mechanism has not been cleared in all aspects but the main features are widely accepted including that nitrate is first converted to nitrite before in a second step two parallel reaction pathways occur, one leading to nitrogen and the other to ammonium [96,99–103]. Eqs. (18)–(20) denote the stoichiometry of these transformations.

$$NO_2^- + H_2 \rightarrow NO_2^- + H_2O \quad (18)$$

$$2NO_2^- + 3H_2 \rightarrow N_2 + 2OH^- + 2H_2O \quad (19)$$

$$NO_2^- + 3H_2 \rightarrow NH_4^+ + 2OH^- \quad (20)$$

It is assumed that in the second step the reaction actually proceeds via nitrous oxide which is adsorbed on the catalyst surface before the branching to ammonium ions and nitrogen takes place. Moreover, dinitrogen monoxide has been identified as an intermediate product of the formation of nitrogen [104–106]. A widely accepted reaction scheme based on this refined stoichiometry is outlined in Fig. 29.

Experiments have shown that for the hydrogenation of nitrate on palladium a second metal is necessary, preferably Cu, Sn or In. In contrast nitrite is hydrogenated also on monometallic palladium [98,102,103], even more selectively than on bimetallic palladium catalysts [103,107]. Mixtures of bimetallic Pd-Cu catalysts and monometallic palladium catalysts have shown a lower ammonium formation than the bimetallic Pd-Cu catalysts alone [101,103]. Compared to Pd-Sn and Pd-In, Pd-Cu catalysts suffer from a higher formation of nitrite as well as from significant amounts of dinitrogen monoxide [98,105,106,108]. Since indium is less common, Pd-Sn seems to be the favourite catalyst system at present.

The activity and selectivity of the catalysts is strongly dependent on the reaction conditions [102,103,109], first of all on the pH value but also on the concentration of dissolved hydrogen, on the temperature and on the nitrate concentration. A high pH value is connected to a poor nitrate removal rate and to a high formation of ammonium. Total saturation of the water with hydrogen gives a high reaction rate but raises to some extent the formation of ammonium [110,111]. Higher temperatures speed up the reaction rate but the formation of ammonium gains most. The selectivity also depends on the nitrate concentration, i.e. a lower concentration of nitrate is in favour of ammonium formation.

In view of the catalyst, the support material, the palladium loading, the ratio of palladium to the

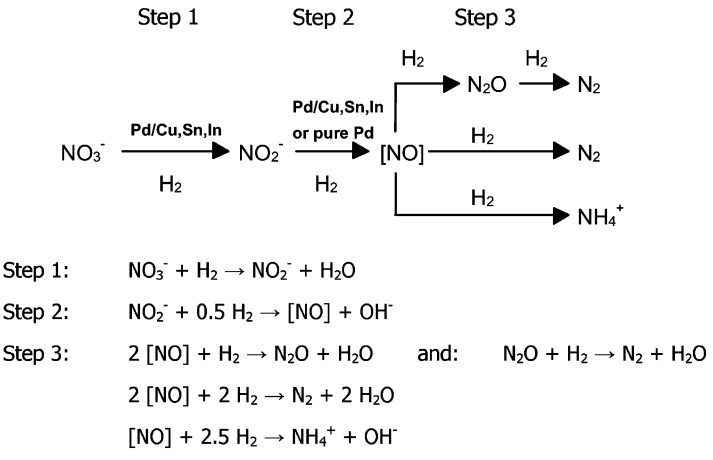

Fig. 29. Reaction scheme and stoichiometry of the hydrogenation of nitrate in water on Pd-Cu and Pd-Sn catalysts [102].

promoter, the size of the metal clusters and the oxidation state of the metals are important for activity and selectivity. We also added the particle size and the pore structure of the support (porosity and pore size distribution) [109]. In most studies γ-alumina supports or silica supports have been used [98,103,110] but zirconia supports were employed as well [111,112]. The demands on the support are manifold. It must provide a reasonably large inner surface area for deposition of the active metals. To facilitate the diffusion the particle size must be small enough, and a high pore volume together with a sufficient fraction of macropores is required. Moreover, the support must be stable against attrition and hydrolysis.

The palladium loading, the palladium to promoter ratio and the particle size of the metals are connected. For each promoter there exists an optimum ratio because the catalyst should have bimetallic metal clusters and monometallic palladium clusters side by side [108,110]. The former are needed to convert nitrate while the latter are more active and selective in converting nitrite. The metal loading and the cluster size together determine the available metal surface area. A high metal surface area in general gives a high reaction rate (if no structure sensitivity of the reaction is observed), but the available inner surface area of the support sets a limit. If the metal loading is too high the average cluster size grows. Hence, an optimum palladium loading exists where the activity per milligram of palladium reaches a maximum.

The influence of the particle size is connected to the formation of hydroxyl anions as the reaction proceeds. If the diffusion inside the catalyst particles is too slow compared to the reaction the produced hydroxyl anions cannot diffuse out fast enough. The consequence is a local pH-increase which reduces the activity and favours the formation of ammonium [102,113]. This can be largely avoided by using extremely fine catalyst particles of a few microns [101]. Moreover, it was shown that pH gradients can be suppressed also by supplying carbon dioxide [98] or by replacing hydrogen as a reducing agent with formic acid [114,115]. Formic acid is decomposed at the catalyst generating hydrogen and carbon dioxide. The released hydrogen reacts with the nitrate while carbon dioxide serves as a buffering agent. Carbon dioxide is readily soluble in water and forms carbonic acid, which in turn dissociates to bicarbonate anions and hydronium ions. A second dissociation equilibrium is effective giving carbonate anions and hydronium ions. Hydronium ions and hydroxyl anions neutralise each other by forming water. Due to the high solubility of carbon dioxide a large amount of hydroxyl anions can be neutralised and so the local pH value remains constant. However, while pH-gradients inside the catalyst may be suppressed by buffering the water with carbon dioxide or by working with formic acid, concentration gradients of nitrate and hydrogen which also occur can be avoided only by using fine catalyst particles (or egg-shell catalysts). Since, fine catalyst particles are difficult to operate on a technical scale attempts have been made to immobilise the catalyst in membranes or in particles with optimised diffusion properties.

- Lüdtke et al. [116] developed catalytic membranes by embedding fine catalyst particles in porous polyetherimide membranes (hollow fibres, sheets). The water was saturated with hydrogen and then passed through the membrane in cross-flow. Due to the short contact time per pass a product recycle was applied.
- Hähnlein et al. [104,117] packed fine catalyst particles into polymer hollow fibres arranged in a hollow fibre module. The water was saturated with hydrogen and then fed to the shell side of the module.
- Prüße et al. [108,118] used fine catalyst particles encapsulated in polyvinyl alcohol (PVAL) hydrogels. The PVAL particles were employed in a conventional reactor with hydrogen saturated feed water.
- Ilinitch et al. [100,119] used asymmetric macroporous alumina membranes as supports. Impregnation methods were applied to deposit the active metals inside the membrane structure. The catalytic membranes were employed in cross-flow with hydrogen saturated water and product recycle similar as in the concept of Lüdtke et al. [116].

We too have proposed asymmetric macroporous ceramic membranes as supports for bimetallic palladium catalysts for nitrate reduction in water [120,121]. This concept was studied in a European research project aimed at the development of catalytic membranes for nitrate removal from drinking water. The active metals were deposited in the fine top layer of the membranes. However, in contrast to the approach followed by Ilinitch we operate the membrane as a *catalytic diffuser*, that is, it serves not only as catalyst support but also as

a dosing device for hydrogen or mixtures of hydrogen and carbon monoxide. The benefit is a better control of the reaction rate and the selectivity. First results of a membrane screening were reported elsewhere [120] as well as information on the preparation of the membranes by metal organic chemical vapour deposition (MOCVD) [121]. In this paper an overview of the experimental results is provided.

3.3. Experimental

3.3.1. Membrane supports

Asymmetric porous alumina membranes obtained from HITK e.V., Hermsdorf (Germany), were used as starting materials. The membranes had an outer diameter of 10 mm and an inner diameter of 7 mm and were cut to a length of 100–120 mm for the preparation and the tests in the membrane reactor. They consist of a coarse α-alumina support, up to two intermediate layers with graded pore size (α-alumina) and a thin top layer made of α-alumina, γ-alumina, titania or zirconia. The top layer was always on the shell side. Its thickness and pore diameter was varied, i.e. α-alumina layers were used with pore diameters of 60–400 nm and thicknesses of 10–50 μm. The zirconia layers had a pore diameter of 65 nm and thicknesses of 10–20 μm. The titania and γ-alumina layers were 0.5 μm thick and had a pore size of 5 nm. All membranes were handled carefully in order to avoid damage of the sensitive top layers.

3.3.2. Preparation methods for placing the catalytic metals in the membrane top layer

To introduce the active metals palladium and tin into the membrane top layer different techniques were used. Initially a very simple impregnation method was applied [120]. In this method a membrane is put on-centre on a rotating shaft. While rotating at 15 rpm the membrane is attached carefully to the surface of a bath containing the metal salts. The bath was prepared by dissolving 166 mg $PdNO_3$ or 40 mg $SnCl_2{\cdot}2H_2O$ in 20 ml twice-distilled water with a few drops of concentrated hydrochloric acid added while gently heating. At a bath temperature of 60°C the impregnation is carried out for about 10 min. Afterwards the membrane is dried in a drying oven at 90°C for 15 min (air) and burned in a laboratory furnace at 400°C for 90 min in air to convert the deposited metal salts into tenacious metal oxides. In the next step the weight increase is determined and it is decided whether a second impregnation step is necessary to achieve the desired metal loading. The deposition of the metals is carried out sequentially. At the end the membrane is burned in air at 500°C in the furnace for 2 h before it is reduced in a hydrogen–nitrogen atmosphere at 350°C for 3 h to obtain the metals in zero oxidation state.

MOCVD was applied as an alternative preparation method using $Pd(II)(hfac)_2$ and $Sn(II)(hfac)_2$ as precursors [121]. The deposition was also carried out sequentially. In case of palladium a pure helium stream is passed through a bed of glass beads containing the palladium precursor which is heated to 80°C. Deposition of tin requires a sublimator temperature of 120°C and a mixture of hydrogen and helium as carrier gas to receive tin in reduced form. The gas stream carrying the precursor vapour is then fed to a heated-wall CVD reactor containing the membrane in central position with the interior sealed so that the precursor can penetrate into the membrane structure only from the shell side. The reactor is kept at 240–250°C and 50 kPa while the deposition is carried out for a predetermined time (derived from the average deposition rate). Calcination and reduction of the prepared membranes is not necessary in MOCVD because the metals are received in reduced form.

About 60 different membranes were prepared according to both methods and tested in screening experiments for their ability to reduce nitrate selectively to nitrogen. The results showed that Pd-Sn on zirconia supports gives the best results. To be able to make a larger number of these membranes with reproducible properties a more sophisticated impregnation apparatus based on a rotational evaporator was designed and built at Venezia Tecnologie, Porto Marghera (Italy), one of the partners in the European project. The membranes from this method were calcined and reduced after the same treatment as the membranes prepared by the simple impregnation technique.

3.3.3. Structural characterisation

The methods applied for characterisation of the structure of the membrane top layers before and after introduction of the catalytic metals, i.e. the pore size, the distribution of the metals and the metal cluster size are described elsewhere [121]. The pore size distribution was measured with a capillary flow porometer.

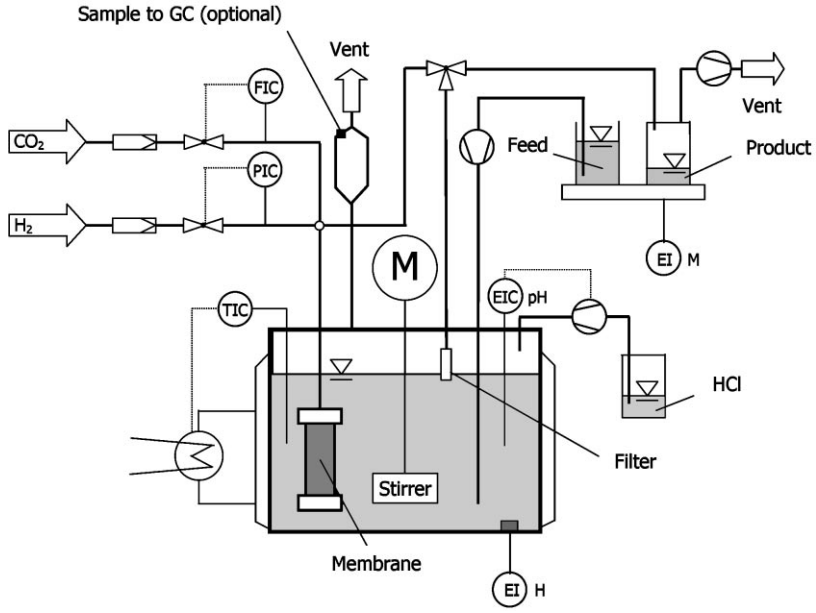

Fig. 30. Basic layout of the laboratory stirred tank membrane reactor — GC: gas chromatograph; M: motor; PIC: pressure controller; FIC: flow controller; TIC: temperature controller; EIC pH: pH control unit (dosage of HCl, optional); EI H: electrochemical sensor for dissolved hydrogen; EI O: optochemical sensor for dissolved oxygen; EI M: balance.

The distribution of the metals was determined by electron probe microanalysis (EPMA/WDX) performed on cross-sectional cuts from different radial and axial positions. The metal cluster size was analysed mainly by X-ray diffraction (XRD/LBA). In addition XPS investigations were carried out at the University of Louvain (Belgium), another project partner, to quantify the palladium to promoter ratio on the catalyst surface.

3.3.4. Catalytic tests

The performance of the catalytic membranes was studied in a stirred-tank membrane reactor with a capacity of 1000 ml (cf. Fig. 30). The reactor was operated mainly in continuous mode. In this set-up a membrane connected to the gas supply line at one end is immersed in the liquid. The other end is sealed. The liquid is mixed by a magnetically coupled blade stirrer. An impeller can be used as well if a good dispersion of the reactor gas in the liquid is desired. However, this is not the case in the catalytic diffuser mode where the gas is supplied to the catalytic layer from inside the membrane tube while not exceeding the bubble point pressure (i.e. no gas bubbles are introduced). A mixture of hydrogen and carbon dioxide is fed to the membrane. For this the desired amount of carbon dioxide is set by a thermal mass flow controller. Hydrogen is fed with the help of a downstream pressure controller which adjusts the hydrogen flow so that a given pressure inside the membrane is reached. The reactor vessel consists of a double-walled glass jacket screwed up between two metal flanges. An electrochemical hydrogen sensor fixed in the bottom flange measures the hydrogen concentration in the liquid. An immersed fibre-optic oxygen sensor is available to detect the concentration of dissolved oxygen. The liquid feed is metered by a pulse-free peristaltic pump, whereas the product is withdrawn by a vacuum pump installed behind the product tank. Before entering the connecting pipe the product stream passes a sintered metal filter to retain fine particles. If necessary the filter can be cleaned by backflushing with hydrogen. For a match of the feed and product flow rates the vacuum pump is adjusted during the experiment based on the reading of a balance recording the combined weight of both tanks. Two separate ion

chromatographs (Metrohm AG, Filderstadt, Germany) are available to analyse the concentration of the anions (nitrate, nitrite) and cations (ammonium), respectively. For measurements without carbon dioxide supply a pH-controller with dosage of hydrochloric acid is available to maintain a constant pH value during the reaction.

The mixing behaviour of the liquid in the reactor corresponds to that of an ideal continuous stirred tank reactor (CSTR), i.e. concentration gradients in the reactor volume can be neglected. This was confirmed by tracer experiments performed before the catalytic tests (displacement technique). No bypassing and no significant dead volume could be detected. Therefore, the nitrate removal rate can be calculated from the CSTR material balance (no volume change) and is related unequivocally to the reactor concentrations measured in the effluent stream. The nitrate removal rate is multiplied with the molecular weight and divided by the palladium loading to give the specific activity of the membrane per unit weight of palladium (mg NO_3^-/mg Pd h), which is an established criterion for comparison of the performance of different catalysts.

$$\text{specific activity} = |R^m_{NO_3^-}| = -\frac{M_{NO_3^-}}{m_{Pd}} \frac{c_{NO_3^-} - c_{NO_3^-,0}}{\tau} \quad (21)$$

The conversion (%) of nitrate and the selectivities to nitrite and ammonium are calculated according to the usual definition based on the measured concentration changes as follows:

$$X_{NO_3^-} = \frac{c_{NO_3^-} - c_{NO_3^-,0}}{c_{NO_3^-,0}} \times 100 \quad (22)$$

$$S_{i,N} = \frac{\dot{n}_i - \dot{n}_{i,0}}{\dot{n}_{NO_3^-,0} - \dot{n}_{NO_3^-}} \frac{\nu_i}{l} \times 100, \quad i = NH_4^+, NO_2^- \quad (23)$$

The selectivity to nitrogen is determined indirectly, i.e. from the material balance for nitrogen atoms.

$$S_{N_2,N} = 100 - \sum_i S_{i,N}, \quad i = NH_4^+, NO_2^- \quad (24)$$

This relies on the assumption that no other nitrogen containing products (e.g. N_2O) are formed. During the membrane screening experiments were performed mostly under the standard testing conditions summarised in Table 4.

Table 4
Standard testing conditions for the screening of the membrane performance (twice-distilled water)

Initial nitrate concentration	100 mg/l
Liquid volume in the reactor	770 ml
Hydrogen pressure in the membrane	400 kPa
Reactor pressure	100 kPa
Carbon dioxide flow through the membrane (supplied together with hydrogen)	(a) 35 ml/min, pH = 4.7
	(b) 0 ml/min, pH control by HCl-dosage
Reactor temperature	15 °C
Residence time	30 min
Stirrer speed	1500 rpm

3.4. Results and discussion

3.4.1. Membrane screening

The top layer of the membrane has two functions. It serves as a support for the active metals and as a contacting region between gas phase and liquid phase. The wetted top layer acts as a barrier for the gas phase, i.e. the gas–liquid interface is established in the pore structure beneath the top layer. This allows to supply hydrogen directly and only to the catalytic region. Bypassing of gas through larger pores (i.e. defects) would lead to the introduction of gas bubbles into the water and is not desired. With reference to the first function the deposition of the metals is aimed at the following features:

- high metal dispersion (small metal clusters);
- desired palladium loading (about 1–5 wt.% based on the top layer);
- desired palladium/promoter ratio (for Pd-Sn catalyst it is around 4);
- uniform distribution of the metals over the top layer;
- deposition of the metals only in the top layer.

Based on the present knowledge about the reaction system this is expected to result in catalytic membranes with good performance for reduction of nitrate.

For what concerns the second function, the screening was performed also to identify operating conditions which allow to maximise the selectivity and activity of the catalytic membranes. In this respect the supply of carbon dioxide together with hydrogen to the catalytic region leads to a much better catalytic performance of the membranes. Hence, membranes with different properties, e.g. prepared by different methods, have to be compared under such operating conditions. The particular advantage of supplying carbon dioxide directly to the reaction zone is that the pH value can be controlled inside the catalytic layer without the need to saturate the whole reactor liquid. Hence, the consumption of carbon dioxide is lower, which also means that less bicarbonate/carbonate is contained in the reactor effluent.

3.4.1.1. Top-layer material, pore size and thickness. Four different commercially available top-layer materials were considered, i.e. α-alumina, γ-alumina, titania and zirconia. The γ-alumina and titania layers are characterised by a small pore diameter of 5 nm and a thickness of only 0.5 μm. Two problems were encountered with these layers. Due to the small pore size during the impregnation a major part of the metals was deposited on top of the layer and not inside the pores. A control of the deposition proved to be difficult. Also in MOCVD the deposition occurred largely on the surface of the layer and was rather irregular. After removal of the adherent metals the membranes showed a poor activity because of the low absolute amount of the catalytic metals. Moreover, it must be assumed that the gas pressure of up to 700 kPa, which was applied in the experiments, was not sufficient to bring the gas–liquid interface close enough to the transition from the intermediate layer to the top layer where the catalyst is located. This is connected to a higher hydrogen mass transfer resistance. Note that, according to Eq. (25) a cylindrical pore with 5 nm diameter has a capillary pressure of 58 MPa at complete wetting ($\sigma = 72.7$ mN/m at 20°C, $\cos\alpha = 1$).

$$p_C = \frac{2\sigma}{r_P}\cos\alpha \tag{25}$$

Due to these problems the investigations were concentrated on α-alumina top layers which were available with pore sizes of 60–400 nm, and with thicknesses from 10 to 50 μm, as well as on zirconia top layers with 65 nm pore size and a thickness of 10–20 μm. These materials were applied successfully for the impregnation and for MOCVD. With zirconia-based Pd-Sn membrane catalysts prepared by MOCVD up to 50% higher activities were detected compared to α-alumina at similar thickness and pore size of the top layer and at comparable metal loading. At the same time the selectivity to nitrogen was reduced only a little, i.e. by not more than 10%.

The variation of the pore size of α-alumina top layers in the range of 60–400 nm caused a moderate change of the specific activity of the Pd-Sn-based membranes. At standard test conditions a weak maximum was noticed around 100 nm. The selectivity did not show a maximum but was reduced slightly with increasing pore size. However, the absolute changes with the pore size are small compared to the fluctuations between the measurement points. The thickness of the α-alumina top layers proved to be more important. For thicknesses up to 20 μm the specific activity at standard test conditions was between 0.8 and 1 mg nitrate per mg palladium per hour. This value dropped

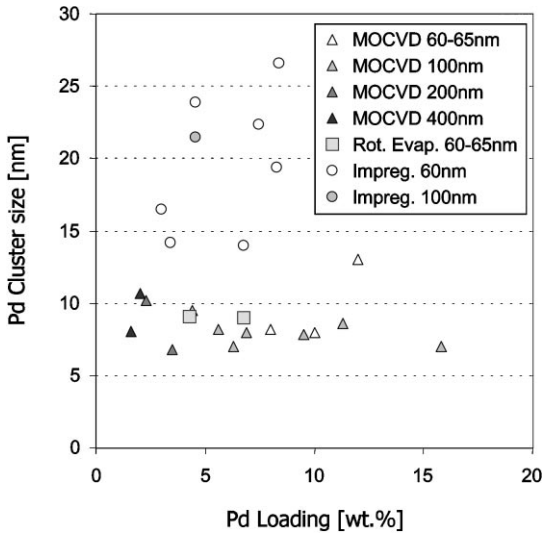

Fig. 31. Palladium cluster size of catalytic membranes prepared by different methods and with different palladium loadings as determined from XRD/LBA; Pd-Sn on α-alumina prepared by simple impregnation and by MOCVD (nominal pore diameter: 60–400 nm; layer thickness: 10–50 μm); Pd-Sn on zirconia prepared by impregnation in the rotational evaporator (nominal pore diameter: 65 nm; layer thickness: 10–20 μm).

to 0.2–0.3 for layers close to 30 μm thickness and above (cf. [121]).

3.4.1.2. Preparation method. Fig. 31 shows the dependency of the palladium cluster size determined by XRD/LBA on the palladium loading for different membranes prepared by the simple impregnation method, by MOCVD and by impregnation in the rotational evaporator. Obviously the simple impregnation leads to a lower dispersion than MOCVD, whereas the modified impregnation in the rotational evaporator gives a similar cluster sizes. Fig. 32 shows an example of the palladium distribution over the membrane cross-section obtained by the different preparation methods. The profiles were determined by EPMA/WDX line scans from three Pd-Sn/ZrO_2 membranes with different palladium loading. The palladium loading based on the weight of the top layer is shown. Regardless of the different absolute values a difference in the characteristics of the three profiles is noticed. The simple impregnation gives the sharpest profile which corresponds to the desired result; almost no palladium is found in the intermediate layer. MOCVD is a bit worse in view of the percentage of the palladium that is trapped in the top layer, and it shows a moderate decrease of the palladium concentration in the top layer inwards. The impregnation in the rotational evaporator causes flat concentration profiles in the top layer, similar as the simple impregnation method, but at the same time the highest palladium concentration of the three methods in the intermediate layer. What is not shown is that the impregnation in the rotational evaporator gives the least deviation between metal profiles taken at different axial and radial positions, whereas MOCVD sometimes leads to large deviations.

Another major difference between the two impregnation methods and MOCVD is connected to the temperature treatment. For Pd-Sn on α-alumina and zirconia it was found that the palladium to tin ratio on the surface detected by XPS is significantly higher when prepared by MOCVD. In all methods palladium was deposited after tin. The average quotient of the Pd/Sn ratio on the surface divided by the Pd/Sn ratio in the bulk (from the weight increase after the preparation) of more than 10 membranes from each method was 1.1 for MOCVD as opposed to 0.3 for both impregnation methods. This means that only in MOCVD the Pd/Sn ratio on the active surface is more or less equal to the bulk value determined by the deposited amount of metals. Membranes prepared by impregnation have a lower palladium concentration on the surface of the bimetallic clusters. Because tin has a much lower melting point than palladium, it is assumed that the high temperature during the calcination and reduction is responsible for an enrichment of tin on the surface. It is also possible that an alloy ($PdSn_3$) is formed.

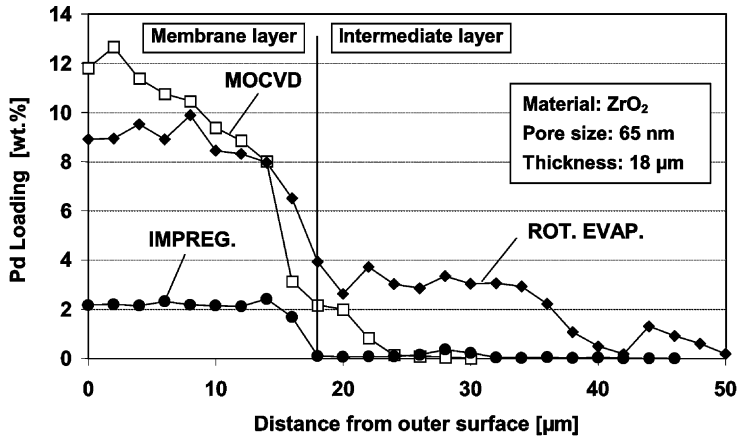

Fig. 32. Palladium concentration profiles from EPMA/WDX over the cross-section of three zirconia-based Pd-Sn membranes prepared according to the different methods, i.e. simple impregnation, MOCVD and impregnation in the rotational evaporator. Influence of the preparation on the penetration depth (vertical line marks the transition from the top layer to the intermediate layer); different palladium loadings.

3.4.1.3. Metal deposition sequence and palladium loading. The sequence of deposition of palladium and tin is important in particular for the preparation by MOCVD where no subsequent high temperature treatment is applied. The calcination at 500°C and the reduction at 350°C after the impregnation probably facilitates the diffusion of tin to the surface, irrespective of whether palladium is on top of tin or vice versa. In contrast, in MOCVD the deposition of palladium after tin (A) should lead to tin clusters partly covered by palladium whereas the opposite sequence (B) should result in palladium clusters covered by tin. If it is true that a good catalyst must have monometallic palladium and bimetallic Pd-Sn clusters side by side, then membrane catalysts prepared after sequence (A) should be more selective than those prepared after (B). The characterisation of the surface composition by XPS has confirmed higher palladium surface concentrations for membranes prepared with the sequence (A) than with sequence (B), and the catalytic experiments have shown that the selectivity of these membranes is higher on the average. Therefore, sequence (A) was applied for all subsequent preparations by MOCVD.

Fig. 33 shows the results obtained under standard test conditions for a variation of the palladium loading from 4 to 16 wt.% (based on the top layer). Pd-Sn/α-alumina membranes are shown with a pore diameter of 100 nm and a top-layer thickness of 20 μm. The Pd/Sn ratio ranged from 3 to 6. A large scattering of the data is obvious which might be due in part to the variation of the Pd/Sn ratio. Despite the scattering it is noticed that the specific activity does not change much while the selectivity to nitrogen is reduced at higher palladium loading. Ammonium formation is the main reason but the selectivity to nitrite is increased likewise at high palladium loading.

The variation of the Pd/Sn ratio is addressed in Fig. 34. Again results for α-alumina-based Pd-Sn membranes with 20 μm thickness and 100 nm pore size of the top layer are shown. The interpretation suffers from a simultaneous change of the palladium loading which varies from 4 to 12 wt.%. However, a tendency can be seen, i.e. that at Pd/Sn ≈ 4 or larger the lowest ammonium formation and the lowest nitrite level is found while the activity is only slightly reduced compared to the activity at lower Pd/Sn ratios.

In conclusion from the results of the membrane screening it can be said that among the two top-layer materials zirconia is favoured. The top-layer thickness should not exceed 20 μm. Suitable pore diameters are in the range of 60–100 nm. The palladium loading should preferably not exceed 5 wt.% in order to maximise the selectivity, and a Pd/Sn ratio around 4–5 is desirable. The simple impregnation method leads to relatively large metal clusters (low dispersion) which are connected to a poor activity. MOCVD in principle has advantages over the impregnation methods. It enables a better control of the deposition beneath the top

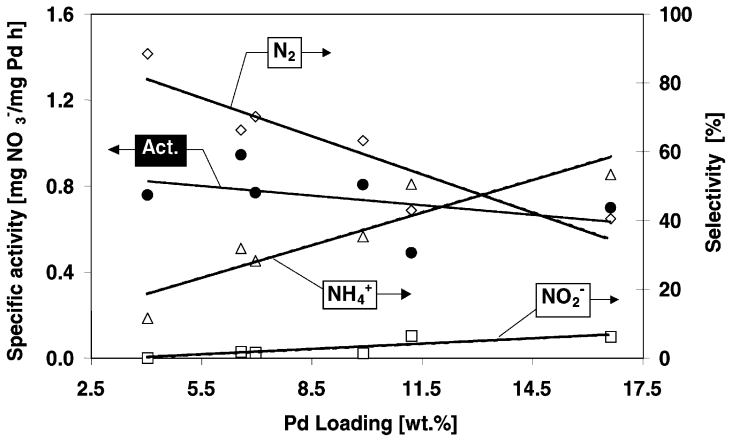

Fig. 33. Influence of the palladium loading on the specific nitrate removal activity and on the selectivity; membrane: Pd-Sn/α-alumina; pore size: 100 nm; top-layer thickness: 20 μm; Pd/Sn ratio: 3/6.

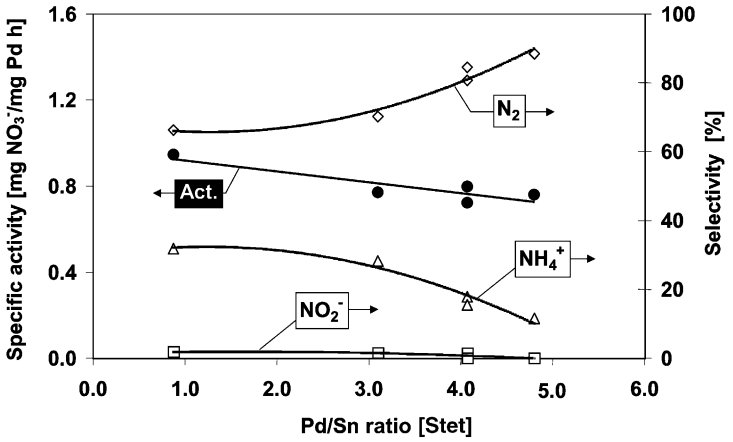

Fig. 34. Dependence of the specific activity and the selectivity on the Pd/Sn ratio; membrane: Pd-Sn/α-alumina; pore size: 100 nm; top-layer thickness: 20 μm; Pd loading: 4–12 wt.% (based on the top layer).

layer compared to the impregnation in the rotational evaporator and it does not lead to an enrichment of tin on the catalytic surface because no temperature treatment is applied. However, given the fact that the uniformity and the reproducibility of the impregnation in the rotational evaporator was the best of all three techniques, this method was selected for the preparation of a larger number of optimised membranes for further kinetic studies on the influence of the important process variables. The properties of these membranes are given in Table 5. They are relatively close to the desired features. Under standard test conditions (cf. Table 4) these membranes reached an average specific activity of 1.7 mg nitrate converted per mg palladium and hour at a selectivity to nitrogen of 91–92%.

3.4.2. *Influence of the main process variables*

With one of the optimised Pd-Sn/ZrO_2 membranes measurements were performed over a period of 3 weeks with intermittent shutdowns overnight and at the weekends. While shutting down the experiment it was tried to avoid a direct contact of the membrane with air over a longer time by storing it in distilled water. Replicate measurements under standard conditions proved that the membrane lost a part of its activity (about 22% in 3 weeks), whereas the selectivity to nitrogen remained constant within the usual fluctuations (88–92%).

Table 5
Properties of the optimised catalytic diffusers prepared by impregnation in the rotational evaporator

Top-layer material	ZrO_2
Nominal pore diameter of the top layer (nm)	65
Nominal thickness of the top layer (μm)	20
Palladium loading (based on the top layer) (wt.%)	6.2
Palladium to tin ratio (weight-based)	2.1
Metal deposition sequence	Pd after Sn
Palladium cluster size (XRD, TEM) (nm)	≈9

3.4.2.1. Carbon dioxide flow through the membrane (pH value). The strong influence of the pH value on the reaction has been mentioned already as well as the effect of the dosage of carbon dioxide. In Fig. 35 the influence of the carbon dioxide volumetric flow rate through the membrane on the specific activity and the selectivity is shown. At zero flow rate, i.e. no buffering in the catalytic layer, the selectivity to nitrogen is only 45% at an activity of 0.75 mg NO_3^-/mg Pd h. The pH value of the reactor liquid is 6.2. Under these conditions nitrite is formed with a relatively high selectivity of 40%. The remaining 15% fall to ammonium. Already at a low carbon dioxide flow rate of 5 ml/min the selectivity to nitrogen rises significantly and the formation of nitrite is more than halved. The pH value in the reactor is reduced to 5.4 and the specific activity is doubled. When, the carbon dioxide flow rate is further increased the increase of the activity begins to level off and finally, at very high carbon dioxide flows, the activity is decreased again. The selectivity to

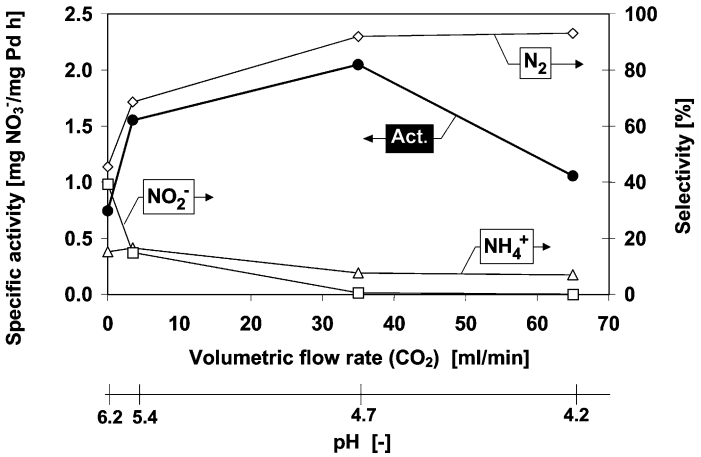

Fig. 35. Influence of the carbon dioxide flow rate through the membrane on the pH value in the reactor liquid and on the catalytic performance; membrane: Pd-Sn/zirconia; pore size: 65 nm; top-layer thickness: 20 μm; Pd/Sn ratio: 2/1.

nitrogen behaves differently: it is increased steadily until it approaches a value of about 95% at very high carbon dioxide flow rates. The highest activity is found at a carbon dioxide flow rate of 35 ml/min. Under these conditions the pH value in the reactor is around 4.7. The selectivity to nitrogen is 89%, nitrite is hardly found, and the remaining 10–11% fall to ammonium. The decrease of the activity at very high carbon dioxide flow rates can be explained by a reduction of the hydrogen partial pressure inside the membrane. This occurs when the carbon dioxide flow rate exceeds the rate at which it is dissolved in the liquid and the carbon dioxide partial pressure is increased at the expense of hydrogen. With significantly reduced hydrogen partial pressure in the gas the reaction rate becomes limited by hydrogen mass transfer.

3.4.2.2. Hydrogen pressure in the membrane. A convenient method to increase the reaction rate is to rise the hydrogen pressure in the membrane. In principle the pressure can be increased up to the bubble point pressure, although the beneficial effect is lost at some point when the hydrogen mass transfer does no longer limit the reaction rate. This behaviour

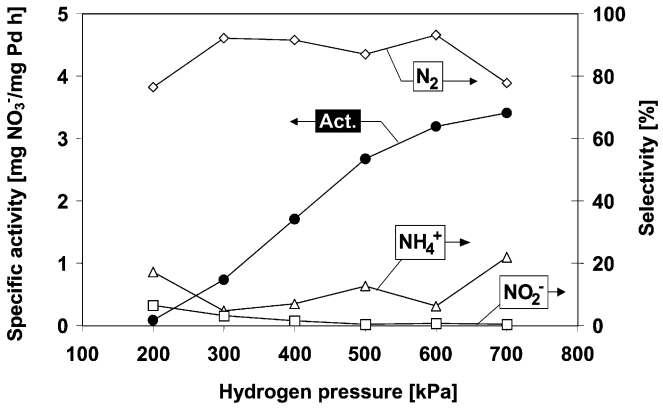

Fig. 36. Effect of the hydrogen pressure in the membrane on the specific activity and on the selectivity; membrane: Pd-Sn/zirconia; pore size: 65 nm; top-layer thickness: 20 μm; Pd/Sn ratio: 2/1; carbon dioxide flow rate: 35 ml/min.

is seen in Fig. 36 from the S-shaped curve giving the specific activity. In view of the deviation of the ammonium selectivity at low and high hydrogen pressure it appears as if the formation of ammonium is not favoured by a higher hydrogen pressure in the investigated pressure range up to 700 kPa, but at further increased hydrogen pressure this could happen. The dissolved hydrogen concentration in the reactor liquid, measured by the electrochemical sensor, was 52 μmol/l for a hydrogen pressure of 200 kPa and 275 μmol/l for 700 kPa. The saturation level at the applied reactor pressure of 100 kPa is 858 μmol/l. This means that even at 700 kPa hydrogen pressure in the membrane only 1/3 of the maximum hydrogen concentration in the reactor liquid is reached. Therefore, an acceleration of the reaction rate seems still possible by further increasing the hydrogen pressure. Besides the increase of the reaction rate the selectivity to nitrite is reduced at higher hydrogen pressure.

3.4.2.3. Reactant concentration (nitrate, nitrite, ammonium). Experiments were carried out with nitrate concentrations in the reactor ranging from 50 to 500 mg/l. The results show that the selectivity is more or less constant in this concentration range. Only at values near 50 mg/l a decrease of the nitrogen selectivity from 90 to 80% in favour of ammonium was noticed. The reaction rate increases with higher nitrate concentration, though not linearly but corresponding to a reaction order of approximately 0.7.

Fig. 37 shows the reaction rate and the selectivity observed in additional experiments with pure nitrite. The overall behaviour is similar as with nitrate, but at comparable reactor concentrations the reaction rate is about three times higher and the selectivity to nitrogen is higher by 10%. Runs with addition of up to 68 mg/l nitrite to the standard amount of 100 mg/l nitrate were also performed. These experiments showed that in presence of nitrite the removal rate of nitrate is reduced with increasing nitrite concentration, and that the removal rate of nitrite is lower than in absence of nitrate. Hence, the reaction rate is not "additive" on the catalyst, but both ions compete for (the same) active sites.

Finally, adding ammonium to the nitrate feed gave a small reduction of the nitrate removal rate by roughly 5%. The formation of nitrite was increased by the same order of magnitude.

3.4.2.4. Temperature. The reaction temperature was varied in the range of 10–55°C. The results are summarised in Fig. 38. The specific activity increases with temperature but the increase becomes smaller at higher temperatures and is almost zero above 40°C. This points to mass transfer limitations which could control the reaction rate at higher temperatures. Above 20°C the formation of ammonium is accelerated more and

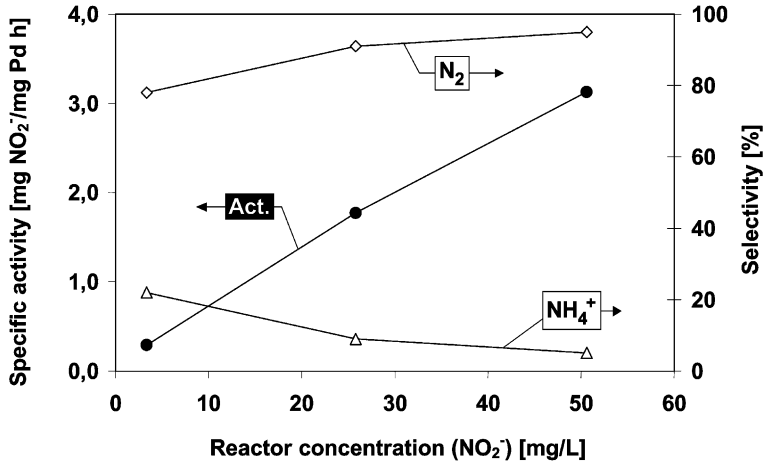

Fig. 37. Influence of the nitrite concentration in the reactor on the specific activity and the selectivity during nitrite removal; membrane: Pd-Sn/zirconia; pore size: 65 nm; top-layer thickness: 20 μm; Pd/Sn ratio: 2/1.

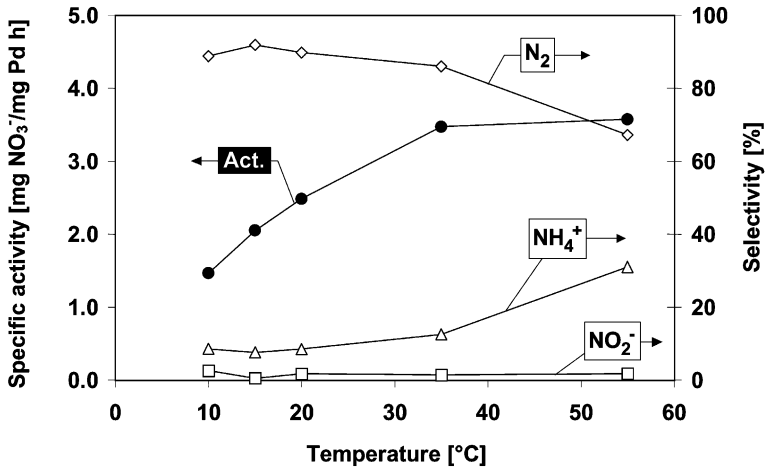

Fig. 38. Temperature dependency of the specific activity and the selectivity; membrane: Pd-Sn/zirconia; pore size: 65 nm; top-layer thickness: 20 μm; Pd/Sn ratio: 2/1.

more at the expense of nitrogen, whereas the net formation rate of nitrite is obviously not affected by the temperature.

3.4.2.5. N_2O formation. The nitrogen selectivities described so far have all been obtained based on the assumption that no N_2O was formed (cf. Eq. (24)). To check this assumption two discontinuous experiments were performed, one with a Pd-Sn/ZrO_2 membrane and one for comparison with a Pd-Cu/ZrO_2 membrane. During these experiments the reactor was set under pressure with a 3:1 mixture of hydrogen and carbon dioxide and then closed. No gas was flown through the membrane, which now acted as one single tubular egg-shell catalyst. Liquid samples and gas samples were drawn off the reactor in certain time intervals and analysed with the ion chromatographs and an additional gas chromatograph (Dani 86.10, TCD) which was prepared for analysis of N_2 and N_2O. These experiments showed that the Pd-Cu-based membrane catalyst produced similar amounts of N_2O and N_2, whereas only N_2 was detected in the gas phase in case of the Pd-Sn membrane catalyst. The error of the nitrogen material balance was similar in both cases, i.e. less than 20% even after 10 h. While these results do not prove in fact that the Pd-Sn-based membrane catalyst does not produce N_2O, because of the high solubility of N_2O in water, they nevertheless show that the N_2O formation is small compared to that of the Pd-Cu catalyst. Similar observations have been reported by Hähnlein [104] and Daum and Vorlop [105].

In conclusion the kinetic experiments have shown that the control of the pH value by dosage of carbon dioxide together with hydrogen through the membrane is the key to a good performance of the optimised Pd-Sn/ZrO_2 membranes. The hydrogen pressure inside the membrane represents the second important operating variable which determines the reaction rate. As long as the nitrate concentration is not too low the selectivity to nitrogen can be maintained relatively high. However, it decreases with lower nitrate concentration, which means that backmixing in an industrial reactor should be avoided. The temperature should be kept as low as possible, but for nitrate reduction in ground and surface water this is probably no issue.

All in all it must be said that the activity of the catalytic diffusers, when operated with carbon dioxide buffering through the membrane, is fairly good. Specific activities between 0.7 and 3.5 mg NO_3^-/mg Pd h and nitrogen selectivities of 82–92% were reached depending on the operating conditions.

4. Critical evaluation and outlook

It has been shown that catalytic membranes with interesting properties can be obtained by introducing palladium and tin in the top layer of asymmetric

porous ceramic membranes, preferentially employing macro/mesoporous α-alumina or zirconia as top-layer materials. These membranes can be used as catalytic diffusers for the hydrogenation of nitrate and nitrite in water. The main advantage of the catalytic diffuser, besides the immobilisation of the active phase, is the possibility to supply the required hydrogen together with carbon dioxide used as a buffering agent directly to the catalytic region. Thereby it is possible not only to diminish the hydrogen mass transfer resistance but also to control the local pH value in the catalytic layer without the need to saturate the whole reactor liquid with carbon dioxide. And it is possible to control the nitrate removal rate by variation of the hydrogen pressure in the membrane, which allows to adjust the reaction rate quickly to changing requirements.

Optimised Pd-Sn/ZrO_2 diffusers prepared by impregnation in a rotational evaporator have shown an average specific activity for nitrate removal of 1.7 mg NO_3^-/mg Pd h in standard tests (twice-distilled water) together with a nitrogen selectivity around 90% at conversions from 15 to 50%. The specific activity for removal of nitrite was three times higher while the nitrogen selectivity under these conditions reached up to 95%. Compared to other approaches aimed at the immobilisation of fine catalyst particles for the reduction of nitrate, e.g. using cross-flow polymer membranes with built in catalyst particles [116], hollow fibres packed with powder catalysts [104,117], PVAL encapsulated catalysts [108,118] and ceramic membranes with impregnated catalytic metals in cross-flow [100,119] these are excellent results. However, the present selectivity to ammonium (6–10%) is still not sufficient for a technical process, where the ammonium level must be kept below 0.5 mg/l.

First experiments with tap water have shown recently that the catalytic diffusers can work also under more realistic operating conditions. However, in presence of large amounts of carbonates/bicarbonates the carbon dioxide buffering through the membrane proved to be less effective, which led to a 20% decrease of the nitrogen selectivity. A good performance over 3 weeks was demonstrated on tap water without carbonates/bicarbonates. It was found that the diffusers are deactivated to some extent in contact with air, and that they can be regenerated by a new reduction in hydrogen containing atmosphere. Moreover, the membranes are able to remove chlorinated hydrocarbons and chlorine containing pesticides from the water very efficiently along with nitrate (reductive dechlorination). An accompanying modelling study was started to assist the interpretation of the experimental results, in particular concerning the interaction of the mass transfer and the reaction kinetics in the catalytic diffuser.

Finally, there seems to be still room for an improvement of the preparation of the catalytic diffusers, i.e. with respect to the metal dispersion, to the support and additional promoters. Therefore, it is believed that this technology could in fact lead to the development of an improved catalytic process for nitrate removal from water supplies.

Acknowledgements

The authors thank all partners of the European research project, Prof. G. Strukul, Dr. M. Marella, Dr. P. Ruiz, Dr. F. Luck, Ir. M. van Donk and Prof. G. Centi for the fruitful co-operation and Mrs. M. Schorr and Mr. M. Jusek (DECHEMA e.V.) for EPMA analysis, pulse CO-chemisorption and XRD measurements. Financial support by the Bavarian Catalysis Research Network FORKAT II and by the European Community is gratefully acknowledged.

References

[1] T.T. Tsotsis, A.M. Champagnie, R.G. Minet, P.K.T. Liu, in: E.R. Becker, C.J. Perreira (Eds.), Computer-Aided Design of Catalysts, Chemical Industries, Vol. 51, Marcel Dekker, New York, 1993 (Chapter 12).
[2] J. Coronas, J. Santamaria, Catal. Today 51 (1999) 377.
[3] G. Saracco, H.W.J.P. Neomagus, G.F. Versteeg, W.P.M. van Swaaij, Chem. Eng. Sci. 54 (1999) 1997.
[4] M. Cheryan, M.A. Mehaia, in: W.C. McGregor (Ed.), Membrane Separations in Biotechnology, Bioprocess Technology, Vol. 1, Marcel Dekker, New York, 1986.
[5] R. Govind, N. Itoh (Eds.), AIChE Symposium Series 268, AIChE, New York, 1989.
[6] J.L. Lòpez, S.L. Matson, T.J. Stanley, J.A. Quinn, in: B. Mattiasson, O. Holst (Eds.), Extractive Bioconversions, Bioprocess Technology, Vol. 11, Marcel Dekker, New York, 1991.
[7] S.L. Matson, J.A. Quinn, in: W.S.W. Ho, K.K. Sirkar (Eds.), The Membrane Handbook, Chapman & Hall, New York, 1992.
[8] J. Zaman, A. Chakma, J. Membr. Sci. 92 (1994) 1.
[9] G. Saracco, V. Speccia, Catal. Rev.-Sci. Eng. 36 (1994) 304.

[10] G. Saracco, G.F. Versteeg, W.P.M. Van Swaaij, J. Membr. Sci. 95 (1994) 105.
[11] G. Saracco, V. Speccia, in: A. Cybulski, J.A. Moulijn (Eds.), Structured Catalysts and Reactors, Vol. 71, Marcel Dekker, New York, 1998 (Chapter 17).
[12] J.N. Armor, Appl. Catal. 69 (1989) 1.
[13] J.N. Armor, Catal. Today 25 (1995) 199.
[14] J.N. Armor, J. Membr. Sci. 147 (1998) 217.
[15] J.L. Falconer, R.D. Noble, D.P. Sperry, in: R.D. Noble, S.A. Stern (Eds.), Membrane Separations Technology. Principles and Applications, Membrane Science and Technology, Vol. 2, Elsevier, Amsterdam, 1995 (Chapter 14).
[16] J. Sanchez, T.T. Tsotsis, in: A.J. Burggraf, L. Cot (Eds.), Fundamentals of Inorganic Membrane Science and Technology, Membrane Science and Technology Series, Vol. 4, Elsevier, Amsterdam, 1996 (Chapter 11).
[17] H.P. Hsieh, Inorganic Membranes for Reaction and Separation, Membrane Science and Technology Series, Vol. 3, Elsevier, Amsterdam, 1996.
[18] J.A. Dalmon, in: H. Knözinger, G. Ertl, J. Weitkamp (Eds.), Handbook of Heterogeneous Catalysis, Vol. 3, Wiley, Weinheim, 1997 (Chapter 5.2.3).
[19] V.M. Gryaznov, N.V. Orekhova, in: A. Cybulski, J.A. Moulijn (Eds.), Structured Catalysts and Reactors, Chemical Industries, Vol. 71, Marcel Dekker, New York, 1998 (Chapter 16).
[20] V.M. Gryaznov, Catal. Today 51 (1999) 351.
[21] K.K. Sirkar, P.V. Shanbhag, A.S. Kovvali, Ind. Eng. Chem. Res. 38 (1999) 3715.
[22] T. Graham, Philos. Trans. R. Soc., Lond. 156 (1866) 39.
[23] G.D. Berkheimer, R.E. Buxbaum, J. Vac. Sci. Technol. A 3 (1985) 412.
[24] J. Shu, B.P.A. Grandjean, A. van Neste, S. Kaliaguine, Can. J. Chem. Eng. 69 (1991) 1036.
[25] G.L. Holleck, J. Phys. Chem. 74 (1970) 503.
[26] A.G. Knapton, Platinum Met. Rev. 21 (1977) 44.
[27] D.T. Hughes, I.R. Harris, Z. Phys. Chem. 117 (1979) 697.
[28] J.E. Philpott, Platinum Met. Rev. 29 (1985) 12.
[29] R.B. Moore, V. Raman, Int. J. Hydrogen Energy 23 (1998) 617.
[30] C. Hsu, R.E. Buxbaum, J. Nucl. Mater. 141 (1986) 238.
[31] Y. Yilidirim, E. Gobina, R. Hughes, J. Membr. Sci. 135 (1997) 107.
[32] J.P. Collins, R.W. Schwartz, R. Sehgal, T.L. Ward, C.J. Brinker, G.P. Hagen, C.A. Udovich, Ind. Eng. Chem. Res. 35 (1996) 4398.
[33] J.K. Ali, E.J. Newson, D.W.T. Rippin, Chem. Eng. Sci. 49 (1994) 2129.
[34] J. Shu, B.P.A. Grandjean, S. Kaliguine, Appl. Catal. A: Gen. 119 (1994) 305.
[35] T.H. Hsiung, D.D. Christman, E.J. Hunter, A.R. Homyak, AIChE J. 45 (1999) 204.
[36] E. Kikuchi, CATTECH 1 (1997) 67.
[37] S. Uemiya, N. Sato, H. Ando, E. Kikuchi, Ind. Eng. Chem. Res. 30 (1991) 589.
[38] A.N. Karanov, V.M. Gryaznov, Kinet. Catal. 25 (1984) 60.
[39] J.C.S. Booth, M.L. Doyle, S.M. Gee, J. Miller, L.-A. Scholtz, P.A. Walker, in: Proceedings of the 11th World Hydrogen Energy Conference, Stuttgart, 23–28 June 1996, p. 867.
[40] G. Alfeld, J. Völkl, Hydrogen in Metals I, Springer, New York, 1978.
[41] R.E. Buxbaum, T.L. Marker, J. Membr. Sci. 85 (1993) 29.
[42] N.M. Peachy, R.C. Snow, J. Membr. Sci. 111 (1996) 123.
[43] A.C. Markrides, M.A. Wright, D.N. Jewett, US Patent 3,350,846 (1967).
[44] D.J. Edlund, J. McCarthy, J. Membr. Sci. 107 (1995) 147.
[45] R.E. Buxbaum, A.B. Kinney, Ind. Eng. Chem. Res. 35 (1996) 530.
[46] G. Xomeritakis, Y.-S. Lin, J. Membr. Sci. 133 (1997) 217.
[47] G. Xomeritakis, Y.-S. Lin, AIChE J. 44 (1998) 174.
[48] V. Jayaraman, Y.-S. Lin, J. Membr. Sci. 104 (1995) 251.
[49] S.-E. Nam, S.-H. Lee, K.-H. Lee, J. Membr. Sci. 153 (1999) 163.
[50] Z.Y. Li, H. Maeda, K. Kusakabe, S. Morooka, H. Anzei, S. Akiyama, J. Membr. Sci. 78 (1993) 247.
[51] S. Uemiya, Sep. Purif. Methods 28 (1999) 51.
[52] J.P. Collins, J.D. Way, US Patent 5,451,386 (1995).
[53] S. Uemiya, N. Sato, H. Ando, Y. Kude, T. Matsuda, E. Kikuchi, J. Membr. Sci. 56 (1991) 303.
[54] R.S. Souleimanova, A.S. Mukasyan, A. Varma, J. Membr. Sci. 166 (2000) 249.
[55] P.P. Mardilovich, Y. Shing, Y.H. Ma, M.-H. Rei, AIChE J. 44 (1998) 310.
[56] K.L. Yeung, A. Varma, AIChE J. 41 (1995) 2131.
[57] A. Li, W. Liang, R. Hughes, Catal. Today 56 (2000) 45.
[58] L.-Q. Wu, N. Xu, J. Shi, AIChE J. 46 (2000) 1075.
[59] L.-Q. Wu, N. Xu, J. Shi, Ind. Eng. Chem. Res. 39 (2000) 342.
[60] P. Quicker, V. Höllein, R. Dittmeyer, Catal. Today 56 (2000) 21.
[61] P. Quicker, Doctoral Thesis, University of Erlangen, 2000.
[62] H. Zhao, K. Pflanz, J.-H. Gu, A.-W. Li, N. Stroh, H. Brunner, G. Xiong, J. Membr. Sci. 142 (1998) 147.
[63] V.M. Gryaznov, O.M. Serebryannikova, Yu.M. Serov, Appl. Catal. A: Gen. 96 (1993) 15.
[64] S. Yan, H. Maeda, K. Kusakabe, S. Morooka, Ind. Eng. Chem. Res. 33 (1994) 616.
[65] S. Morooka, S. Yan, S. Yokoyama, K. Kusakabe, Sep. Sci. Technol. 30 (1995) 2877.
[66] K. Kusakabe, S. Yokoyama, S. Morooka, J.-I. Hayashi, H. Nagata, Chem. Eng. Sci. 51 (1996) 3027.
[67] S. Uemiya, M. Kajiwara, T. Kojima, AIChE J. 43 (1997) 2715.
[68] E. Kikuchi, S. Uemiya, Gas Sep. Purif. 5 (1991) 261.
[69] N. Jemaa, J. Shu, S. Kaliaguine, B.P.A. Grandjean, Ind. Eng. Chem. Res. 35 (1996) 973.
[70] A. Li, W. Liang, R. Hughes, J. Membr. Sci. 149 (1998) 259.
[71] J.P. Collins, J.D. Way, Ind. Eng. Chem. Res. 32 (1993) 3006.
[72] S. Uemiya, Y. Kude, K. Sugino, N. Sato, T. Matsuda, E. Kikuchi, Chem. Lett. (1988) 1687.
[73] V. Höllein, M. Thornton, R. Dittmeyer, Catal. Today 67 (2001) 33.
[74] H. Weyten, J. Luyten, K. Keizer, L. Willems, R. Leysen, Catal. Today 56 (2000) 3.

[75] S.N. Paglieri, K.Y. Foo, J.D. Way, J.P. Collins, D.L. Harper-Nixon, Ind. Eng. Chem. Res. 38 (1999) 1925.
[76] S. Uemiya, N. Sato, H. Ando, T. Matsuda, E. Kikuchi, Appl. Catal. 67 (1991) 223.
[77] A. Li, W. Liang, R. Hughes, J. Membr. Sci. 165 (2000) 135.
[78] N. Itoh, W. Xu, K. Haraya, J. Membr. Sci. 66 (1992) 149.
[79] R.E. Buxbaum, A.B. Kinney, Ind. Eng. Chem. Res. 35 (1996) 530.
[80] T.M. Raybold, M.C. Huff, Catal. Today 56 (2000) 35.
[81] M. Tsapatsis, G.R. Gavalas, G. Xomeritakis, in: N.N. Kanellopoulos (Ed.), Recent Advances in Gas Separation by Microporous Ceramic Membranes, Membrane Science and Technology Series, Vol. 6, Elsevier, Amsterdam, 2000 (Chapter 3.4).
[82] E. Wicke, H. Brodowsky, in: G. Alefeld, J. Völkl (Eds.), Hydrogen in Metals II, Springer, Berlin, 1978 (Chapter 3.5).
[83] R. Dittmeyer, V. Höllein, P. Quicker, G. Emig, G. Hausinger, F. Schmidt, Chem. Eng. Sci. 54 (1999) 1431.
[84] B.J. Wood, J. Catal. 11 (1968) 30.
[85] N. Itoh, AIChE J. 33 (1987) 1576.
[86] N. Itoh, Catal. Today 25 (1995) 351.
[87] N. Itoh, T.-H. Wu, J. Membr. Sci. 124 (1997) 213.
[88] J.K. Ali, A. Baiker, Appl. Catal. A: Gen. 155 (1997) 41.
[89] J.K. Ali, D.W.T. Rippin, Sep. Sci. Technol. 29 (18) (1994) 2475.
[90] M. Sheintuch, R.M. Dessau, Chem. Eng. Sci. 51 (1996) 535.
[91] H. Weyten, K. Keizer, A. Kinoo, J. Luyten, R. Leysen, AIChE J. 43 (1997) 1819.
[92] Y. She, J. Han, Y.H. Ma, in: Proceedings of the 4th International Conference on Catalysis in Membrane Reactors, Zaragoza, Spain, 3–5 July 2000, p. 61.
[93] Gutec GmbH, German Patent DE 3 830 850 (1988).
[94] K.-D. Vorlop, T. Tacke, Chem. Ing. Tech. 61 (1989) 836.
[95] Solvay Umweltchemie GmbH, European Patent 0 359 074 (1989).
[96] K.-D. Vorlop, Jahrbuch Biotechnologie 4 (1992) 307.
[97] M. Sell, M. Bischoff, D. Bonse, Vom Wasser 79 (1992) 129.
[98] A. Lecloux, Catal. Today 53 (1999) 23.
[99] J. Wärnå, I. Turunen, T. Salmi, T. Maunula, Chem. Eng. Sci. 49 (1994) 5763.
[100] O.M. Ilinitch, F.P. Cuperus, V.V. Gorodetskii, M.Yu. Smirnov, O.P. Burmatova, I.O. Ilinitch, in: Proceedings of the 4th ESF Workshop on Catalytic Membranes, Oslo, Norway, 30 May–1 June, 1997, p. 89.
[101] M. Hähnlein, U. Prüße, S. Hörold, K.-D. Vorlop, Chem. Ing. Tech. 69 (1997) 93.
[102] T. Tacke, Doctoral Thesis, University of Braunschweig, 1991.
[103] S. Hörold, Doctoral Thesis, University of Braunschweig, 1995.
[104] M. Hähnlein, Doctoral Thesis, University of Braunschweig, 1999.
[105] J. Daum, K.-D. Vorlop, Chem. Ing. Tech. 70 (1998) 1567.
[106] J. Daum, K.-D. Vorlop, Chem. Eng. Technol. 22 (1999) 199.
[107] A. Pintar, J. Battista, J. Levec, Water Sci. Tech. 37 (1998) 177.
[108] U. Prüße, Doctoral Thesis, University of Braunschweig, 1999.
[109] A. Pintar, J. Batista, J. Levec, T. Kajiuchi, Appl. Catal. B: Environ. 11 (1996) 81.
[110] S. Hörold, K.-D. Vorlop, T. Tacke, M. Sell, Catal. Today 17 (1993) 21.
[111] G. Strukul, F. Pinna, M. Marella, L. Meregalli, M. Tomaselli, Catal. Today 27 (1996) 209.
[112] G. Strukul, R. Gavagnin, F. Pinna, E. Modaferri, S. Perathoner, G. Centi, M. Marella, M. Tomaselli, Catal. Today 55 (2000) 139.
[113] F. Fergg, F.J. Keil, Comp. Chem. Eng. 22 (1998) 611.
[114] U. Prüße, M. Kröger, K.-D. Vorlop, Chem. Ing. Tech. 69 (1997) 87.
[115] U. Prüße, M. Hähnlein, J. Daum, K.-D. Vorlop, Catal. Today 55 (2000) 79.
[116] K. Lüdtke, K.-V. Peinemann, R.-D. Behling, J. Membr. Sci. 151 (1998) 3.
[117] M. Hähnlein, U. Prüße, J. Daum, V. Morawsky, M. Kröger, M. Schröder, M. Schnabel, K.-D. Vorlop, in: B. Delmon, P.A. Jacobs, R. Maggi, J.A. Martens, P. Grange, G. Poncelet (Eds.), Studies of Surface Science and Catalysis, Vol. 118, Preprint Catalysis VII, Elsevier, Amsterdam, 1998, p. 99.
[118] U. Prüße, V. Moravsky, A. Dierich, A. Vaccaro, K.-D. Vorlop, in: B. Delmon, P.A. Jacobs, R. Maggi, J.A. Martens, P. Grange, G. Poncelet (Eds.), Studies of Surface Science and Catalysis, Vol. 118, Preprint Catalysis VII, Elsevier, Amsterdam, 1998, p. 137.
[119] O.M. Ilinitch, P.F. Cuperus, L.V. Nosova, E.N. Gribov, Catal. Today 56 (2000) 137.
[120] K. Daub, G. Emig, M.-J. Chollier, M. Callant, R. Dittmeyer, Chem. Eng. Sci. 54 (1999) 1577.
[121] K. Daub, V.K. Wunder, R. Dittmeyer, Catal. Today, 67 (2001) 257.